Abdoul-Baki Tchakpedeou[1]
Solar Energy Laboratory (LES),
Department of Physics,
Faculty of Sciences (FDS),
Regional Center of Excellence for Electricity
Management (CERME),
University of Lome,
01.B.P: 1515, Lome, Togo
e-mail: abdoul-baki.tchakpedeou@univ-lome.tg

Yendoubé Lare
Associate Professor
Solar Energy Laboratory (LES),
Department of Physics,
Faculty of Sciences (FDS),
Regional Center of Excellence for Electricity
Management (CERME),
University of Lome,
01.B.P: 1515, Lome, Togo
e-mail: yenlare@univ-lome.tg

Kossi Napo
Professor
Solar Energy Laboratory (LES),
Department of Physics,
Faculty of Sciences (FDS),
Regional Center of Excellence for Electricity
Management (CERME),
University of Lome,
01.B.P: 1515, Lome, Togo
e-mail: silnapo@yahoo.fr

Arafat Fousseni
Solar Energy Laboratory (LES),
Department of Physics,
Faculty of Sciences (FDS),
University of Lome,
01.B.P: 1515, Lome, Togo
e-mail: araf.fousseni@gmail.com

An Improved Levenberg– Marquardt Approach With a New Reduced Form for the Identification of Parameters of the One-Diode Photovoltaic Model

Building a highly accurate model for solar cells and photovoltaic (PV) modules based on experimental data is becoming increasingly important for the simulation, evaluation, control, and optimization of PV systems. Powerful, accurate, and more robust optimization algorithms are needed to solve this problem. In this study, a new optimization approach based on the Levenberg–Marquardt algorithm (ImLM) is proposed to estimate the parameters of PV cells and modules and simulate their electrical behavior under all environmental conditions efficiently and accurately. To avoid the premature convergence of the Levenberg–Marquardt algorithm and the long computation time caused by a bad choice of initial values, we propose a new approach. This is a new reduced form leading to a nonlinear relationship of the series resistance and thus allowing to calculate the optimal initial values of the model parameters. Comparisons with other published methods show that the proposed approach gives not only a more accurate final solution but also a fast convergence speed and a better stability. Furthermore, tests on three PV modules of different technologies (multi-crystalline, thin film, and monocrystalline) reveal that the proposed algorithm performs well at different irradiations and temperatures. These results confirm that the ImLM approach is a valuable tool and can be an effective and efficient alternative for extracting PV model parameters and simulating PV module behavior under different conditions. [DOI: 10.1115/1.4053624]

Keywords: photovoltaic models, parameter extraction, Levenberg–Marquardt algorithm, new reduced form, statistical analysis

1 Introduction

Due to the major global energy and environmental challenges, the development of renewable energy sources, such as solar, wind, wave, nuclear, tidal, geothermal, biomass, and so on, has attracted a lot of attention in developing countries and is emerging as an unavoidable alternative for power generation [1–3]. Among these renewable energy sources, solar seems to be the most promising. This source is attracting a lot of interest because of its easy installation and the important characteristics it combines, such as high scalability, lack of direct pollution, and dependence on inexhaustible solar radiation, available at different levels but all over the world [4,5]. Solar photovoltaic systems, which can directly convert solar energy into electricity, have been deployed worldwide after experiencing strong growth in recent years [6–8]. However, the energy productivity of a photovoltaic (PV) system is strongly influenced by several external environmental factors, including temperature, solar radiation (solar energy and spectrum), soiling, shading, and aging [9–11].

A PV system contains different parts centered around a solar panel which typically has arrays of interconnected solar cells.

Building a highly accurate mathematical model to describe the nonlinear current–voltage (I–V) relationship of solar cells is a fundamentally important task for the design, simulation, evaluation, analysis, control, and optimization of PV systems [6,12–14]. Many works have developed several models of electrical circuits with different levels of complexity. Among these models, the two-diode model (2DM) is known to be the most appropriate to represent the equivalent electrical circuit of a P–V system [13]. However, this model is further complicated by the fact that its execution time is long, and its various parameters (seven in total) are nonlinear. Thus, the one-diode model (1DM) is the most popular and widely used model because it offers a reasonable compromise in terms of simplicity, accuracy, and execution speed [15]. The main parameters involved in the 1DM include the generated photocurrent, saturation current, series resistance, shunt resistance, and ideality factor, which must be determined based on the available information.

The parameters that characterize the electrical model can be estimated from the information in the datasheet provided by the manufacturers [16] or from a current–voltage (I–V) curve measured experimentally on the PV source [17,18]. Typically, the datasheet only includes information about the short circuit, open circuit, and maximum power points of the I–V curve verified under standard test conditions (STC). As a result, datasheet-based methods are therefore fundamental for PV system design [15,19]. They are typically characterized by analytical equations, which can be solved sequentially or iteratively [15,19,20]. In contrast, methods

---

based on experimental data from the PV source are essential for studies involving the design of more efficient PV components and the evaluation of aging effects on their performance [21]. Parameter extraction is usually transformed into an optimization problem that is continuous, multidimensional, constrained, highly nonlinear, and multimodal in nature. Thus, PV parameter extraction methods are generally grouped into three categories: analytical methods, numerical methods, and hybrid methods.

Analytical methods use elementary mathematical formulations based on approximations and simplifying assumptions to obtain the parameters of the electrical model from a few pivot points of the I–V and P–V curves as well as the slopes of these curves at the intersections of the axes [22]. Their main advantages are simplicity, computational efficiency, and ease of implementation. In addition, only one iteration is required to obtain the desired result. However, the quality of the solution is highly dependent on the accuracy of the selected data points [23]. A misallocation of these points or a small error on them can lead to large deviations on these parameters [24,25]. These methods are only suitable for standard test conditions and break down with variations in conditions. In Ref. [26], a Pàde approximant (PA) method is proposed to express the exponential function of the I–V characteristic equation of the 1DM model, and then, an explicit analytical description of the current is obtained. In Ref. [27], an analytical method based on the use of the W-Lambert function is proposed and used to extract various parameters of PV cells. Other analytical approaches such as Taylor series expansion [28,29], approximate explicit equation set-based approach [30], and curve-fitting approaches [16] have been reported in the literature.

Numerical methods consider all measured I–V data points leading to a system of nonlinear equations. Optimization algorithms are implemented to solve this system of equations and thus obtain the electrical model parameters. These optimization algorithms include deterministic methods [31–33] and metaheuristic methods [34–36]. The main advantage of numerical methods, compared to analytical methods, is the ability to obtain more accurate values of the PV model parameters. However, deterministic methods have intrinsic limitations such as the need for continuity, convexity, and differentiability conditions, heavy computations, high sensitivity to initial values, and often lead to local optima [37–39]. In addition, the execution time is longer [40]. Some metaheuristic methods can also easily fall into local minima. Moreover, their performance is highly dependent on the proper setting of the control parameters. Any wrong choice can lead to slow convergence and premature termination of the program [41].

Recently developed hybrid methods [40,42–44] are obtained by combining different optimization algorithms or by integrating different types of methodologies (analytical and numerical). They were introduced to take advantage of the efficiency of numerical methods and the simplicity of analytical approaches and can provide significantly better performance than the other two methods. However, despite their performance in global search, they require the adjustment of several parameters that significantly affect the efficiency and accuracy of the algorithm [45]. Various hybrid methods have been used to solve the PV parameter problem. A cuckoo search algorithm hybridizing with biogeography-based optimization (BHCS) was proposed in Ref. [42] to estimate the PV model parameters. The method proposed by these authors used a heterogeneous cuckoo search strategy and a biogeography-based discovery operator to balance exploration and exploitation. A hybrid floral pollination algorithm was developed in Ref. [46] and is used to estimate the parameters of 1DM and 2DM models. The authors used the same method to extract the parameters of three different types of photovoltaic modules (multi-crystalline, thin film, and monocrystalline). In Ref. [47], a new hybrid methodology that combines the diversification and intensification mechanisms of different metaheuristics (MH) is used to accurately estimate the PV parameters. The proposed methodology can adapt to the specific optimization problem and maintain diversity during solution construction, thus

mitigating premature convergence and population stagnation. In Ref. [48], a novel spiral leader particle swarm optimization (M-SLPSO) algorithm is proposed to solve the PV parameter identification problem. The proposed algorithm uses multiple swarms with different search mechanisms: each swarm is guided by a leader with a different spiral trajectory.

Although many different methods have been proposed to solve the PV parameter extraction problem and several of them give excellent results, the search for competitive algorithms based on different mechanisms remains an important issue. Moreover, most of these methods, mainly iterative methods such as the Levenberg–Marquardt (LM) algorithm, require the initial values. In general, the user gives these initial values intuitively. Then, if the input values are far from the real initial values, the computation time of the algorithm will be long or, at worst, there will be a convergence problem. Even though all the parameters of the PV model impact the electrical behavior of a PV source in some way, a study [49,50] showed that the I–V characteristic of a PV source is much more sensitive to the values of the ideality factor and series resistance. Special attention should be paid to the initial estimation of ideality factor and series resistance when implementing the derived equations. A method for obtaining these initial values would be desirable, as the accuracy of the algorithm, its convergence, and computational time can be affected by inappropriate initial values.

In this paper, a new approach (ImLM) based on the LM algorithm is proposed for simulating the behavior of PV cells and modules under all environmental conditions. This method results from the combination of the traditional LM algorithm and a new reduced form (NRF). NRF is a method based on analytical manipulation leading to a nonlinear equation between the series resistance Rs and the ideality factor n and is used to generate the values of the five parameters of the 1DM5P model from measured I–V data. Then, these parameters value are used to initialize LM algorithm.

The main contributions of this paper are summarized as follows:

- Proposal of a new hybrid ImLM approach with analytical and deterministic principles for the identification of PV parameters and simulate the behavior of PV cells and modules in all environmental conditions.
- The ImLM approach is expected to help improve the accuracy of the LM algorithm and save valuable computation time.
- The performance of ImLM has been extensively studied by applying it to different problems, and the results have shown high accuracy, reliability, and robustness.

The rest of this paper is structured as follows: Sec. 2 describes the mathematical model of the solar cell/P–V module parameter estimation problem; Sec. 3 presents the proposed hybrid algorithm in detail, followed by the experiments, discussions, and comparisons with other published technologies in Sec. 4. Finally, Sec. 5 concludes this paper.

2 Photovoltaic Generator Modeling

In the literature, there exist several PV models that have been introduced to describe the I–V characteristics of the solar cells and PV modules. However, given the high agreement between simplicity, accuracy, and computational speed, the one-diode, five-parameter model is by far the most popular [15,51]. In this section, this model and the PV module are briefly described.

2.1 Photovoltaic Cell Modeling.
The structure of the single-diode model is described as Fig. 1.

In this model, by applying Kirchhoff's law, the output current of the PV cell can be formulated as follows [52]:

$$I = I_{ph} - I_d - I_p \qquad (1)$$
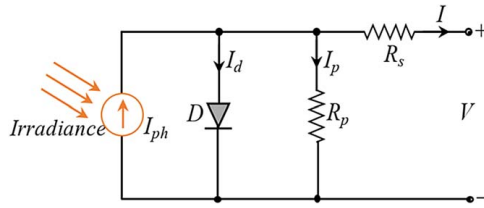
Fig. 1 Equivalent circuit of single-diode model

where I is the cell output current, I_{ph} is the photogenerated current, I_d is the diode current, and I_p is the shunt resistor current.

According to the Shockley equation, I_d can be calculated as

$$I_d = I_0 \left[\exp\left(\frac{V + R_s I}{n V_t} \right) - 1 \right] \tag{2}$$

where I_0 is the reverse saturation current of the diode, V is the cell output voltage, n is the diode ideality factor, R_s is the series resistance, and V_t is the thermal voltage given by expression (3)

$$V_t = \frac{kT}{q} \tag{3}$$

where k is the Boltzmann constant ($1.3806503 \cdot 10^{-23}$ J/K), q is the charge of the elementals ($1.60217646 \cdot 10^{-19}$ C), and T is the temperature of the cell (K).

The shunt current Ip is formulated as follows:

$$I_p = \frac{V + R_s I}{R_p} \tag{4}$$

where R_p is the shunt resistance.

Substituting Eqs. (2) and (4) for Eq. (1), the current–voltage relationship of the one-diode model can be expressed as follows:

$$I = I_{ph} - I_0 \left[\exp\left(\frac{V + R_s I}{n V_t} \right) - 1 \right] - \frac{V + R_s I}{R_p} \tag{5}$$

This model contains a total of five unknown parameters to be estimated (I_{ph}, I_0, R_s, R_p, and n).

2.2 Photovoltaic Module Model. Photovoltaic modules, for the most part, are generally composed of multiple solar cells connected in series and/or parallel. The equivalent circuit model of the PV module is shown in Fig. 2.

The current–voltage relationship can be expressed by Eq. (6) [53–55]

$$I = N_p I_{ph} - N_p I_0 \left[\exp\left(\frac{V + R_s \left(\frac{N_s}{N_p} \right) I}{N_s n V_t} \right) - 1 \right] - \frac{V + R_s \left(\frac{N_s}{N_p} \right) I}{R_p \left(\frac{N_s}{N_p} \right)} \tag{6}$$

where N_p is the number of solar cells in parallel, and N_s is the number of solar cells in series. For the PV module, five
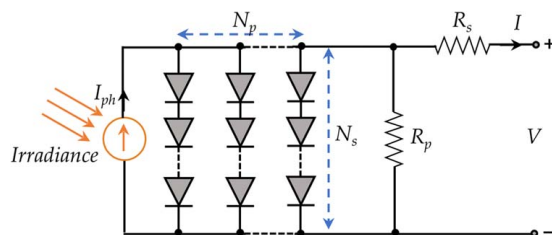
Fig. 2 Equivalent circuit of PV module model

unknown parameters also need to be extracted, namely I_{ph}, I_0, R_s, R_p, and n.

3 Methodology Overview

3.1 Problem Formulation. For the PV model parameters extraction problem, the main objective is to extract a set of parameters that minimize the error between the measured and simulated currents using a performance indicator as an objective function. The performance indicator commonly used in the literature to solve this problem, and which is adopted in this study is the root-mean-square error (RMSE).

For this purpose, to overcome the constraints related to the output current equation, the ImLM approach was used to calculate the simulated current $Ith(V_i, p)$ from the p-parameters of 1DM5P with $p = [I_{ph}, I_0, n, R_s, R_p]$. The current values were determined by solving the equation $Ith(V_i, p) = L_p(V_i)$. For each value V_i of the measured voltage, $L_p(V_i)$ is given by

$$L_p(V_i)$$
$$= \left(I_{ph} - I_0 \left[\exp\left(\frac{V_i + R_s Ith(V_i, p)}{n V_t} \right) - 1 \right] - \frac{V_i + R_s Ith(V_i, p)}{R_p} \right) \tag{7}$$

Then, a vector of residuals or absolute error vector $r(p)$ is obtained from the theoretical current Ith and the measured current I as shown by expression (8)

$$r(p) = \begin{pmatrix} Ith(V_1, p) - I(V_1) \\ Ith(V_2, p) - I(V_2) \\ . \\ . \\ . \\ Ith(V_m, p) - I(V_m) \end{pmatrix} \tag{8}$$

The norm $f(p)$ of the vector $r(p)$ of residuals and the RMSE are determined from the relations (9) and (10), respectively

$$f(p) = \frac{1}{2} \sum_{i=1}^{m} [r_i(p)]^2 \tag{9}$$

$$\text{RMSE}(p) = \sqrt{ \frac{1}{N} \sum_{i=1}^{N} [I(V_i) - Ith(V_i, p)]^2 } = \sqrt{ \frac{2}{N} f(p) } \tag{10}$$

Finally, then, the parameter estimation problem is to find the optimal parameter vector p that minimizes the RMSE and is expressed as follows:

$$Min\ RMSE(p) = Min \sqrt{ \frac{1}{m} \sum_{i=1}^{m} [I(V_i) - Ith(V_i, p)]^2 } = Min \sqrt{ \frac{2}{m} f(p) } \tag{11}$$

where m is the number of empirical points (I_i, V_i) measured with $i \in \mathbb{N}$.

Obviously, a smaller objective function value corresponds to better-estimated parameters. Because of the objective function is nonlinear and transcendental, this problem is difficult to solve.

3.2 Levenberg–Marquardt Method. LM method belongs to this range of nonlinear least-squares optimization algorithms. It is particularly robust and efficient in local (possibly global) search and has become a benchmark algorithm for minimizing continuous twice derivable functions [56]. The LM method has the advantage of combining the behaviors of two gradient-based methods of

different orders and complementary characteristics: the gradient descent method and the Gauss–Newton method [57].

The optimal parameters are obtained after several iterations. For each iteration k, the norm $f(p)$ of the residual vector $r(p)$ and the Jacobian $J(p)$ of $r(p)$ are calculated using the following expressions (12):

$$J(p) = \left[\frac{\partial r(p)}{\partial p}\right] \qquad (12)$$

The gradient ∇f and the Hessian H of $f(p)$ can be estimated by the following expressions (13) and (14), respectively

$$\Delta f = J^T r(p) \qquad (13)$$

$$H = J^T J(p) \qquad (14)$$

Knowing the vector p_k of the parameters at iteration k, the vector p_{k+1} of the parameters at iteration $(k+1)$ is obtained using expression (15)

$$p_{k+1} = p_k - [H_k + \lambda diag(H_k)]^{-1} \nabla f(p_k) \qquad (15)$$

where the positive damping factor λ represents a Lagrange multiplier and is adjusted at each new iteration. It is used to control the speed of convergence. Moreover, the parameter λ varies in the same direction as the error to adjust the influence of the Hessian $H(p)$, on the convergence of the solution. The strategy for regulating the damping factor λ of the Levenberg–Marquardt algorithm is based on the following principle:

If $f(p_{k+1}) > f(p_k)$ then $\lambda = \lambda/10$. Otherwise, $\lambda = 10\lambda$ and $p_{k+1} = p_k$.

The Levenberg–Marquardt algorithm is particularly robust, in the sense that it converges with far fewer iterations and is the benchmark optimization algorithm for many software programs in scientific computing. This robustness is also related to the fact that the term $[H + \lambda \cdot diag(H)]$ is systematically positive. However, the convergence of the algorithm (LM) to the approximate solution is very dependent on the choice of the initial value of the parameters to be optimized. Poor initial values can sometimes lead to premature divergence or convergence of the LM algorithm [32,48]. To overcome this drawback, an analytical technique called new reduced form and based on Brent's algorithm is used to compute the $P_{initial}$ parameters $P_{initial}$ (I_{phin}, I_{0in}, n_{in}, R_{sin}, and R_{pin}) that will be used to initialize the iterative LM algorithm.

3.3 New Reduced Form. NRF is an analytical technique performed in a few computational steps that estimates the five physical parameters of PV modules from their experimental current–voltage characteristics using the diode equivalent circuit model. It requires only limited information from the experimental I–V curve, namely the open circuit voltage (V_{oc}), the short-circuit current (I_{sc}), and the voltage (V_{mp}) and current (I_{mp}) at the maximum power point (MPP).

3.3.1 The Basic Equations. NRF is based on a few equations obtained using the properties of the short circuit, maximum power, and open circuit points leading to the first three equations below

(1) At the open circuit point ($V = V_{oc}$, $I = 0$), we derive

$$0 = N_p I_{ph} - N_p I_0 \left[\exp\left(\frac{V_{oc}}{N_s n V_t}\right) - 1\right] - \left(\frac{N_p}{N_s}\right) \frac{V_{oc}}{R_p} \qquad (16)$$

(2) At the point of short circuit ($V = 0$, $I = I_{sc}$), I_{sc} is calculated by

$$I_{sc} = N_p I_{ph} - N_{par} I_0 \left[\exp\left(\frac{R_s I_{sc}}{N_p n V_t}\right) - 1\right] - \frac{R_s I_{sc}}{R_p} \qquad (17)$$

(3) At the point of maximum power ($V = V_{mp}$, $I = I_{mp}$); therefore, $P = P_{\max}$

$$I_{mp} = N_p I_{ph} - N_p I_0 \left[\exp\left(\frac{1}{n V_t}\left(\frac{V_{mp}}{N_s} + R_s \frac{I_{mp}}{N_p}\right)\right) - 1\right]$$
$$- \frac{N_p}{R_p}\left(\frac{V_{mp}}{N_s} + R_s \frac{I_{mp}}{N_p}\right) \qquad (18)$$

One of the properties of the photovoltaic cell is that its total internal resistance R_T corresponds to the resistance R_L of the external load when the system is operating at its maximum power [58]

$$P = P_{\max} \implies R_T = R_L = \frac{V_{mp}}{N_s}\frac{N_p}{I_{mp}} \qquad (19)$$

Thus, whatever the temperature and irradiation conditions, at the point of maximum power and when the load resistance is exactly matched to the total internal resistance of the cell, we can write

$$R_T = R_s + \frac{R_D R_p}{R_D + R_p} = \frac{V_{mp}}{N_s}\frac{N_p}{I_{mp}} \qquad (20)$$

This expression (20) can be put in the form

$$\frac{1}{R_D} = \frac{\dfrac{I_{mp}}{N_p} + \dfrac{R_s}{R_p}\dfrac{I_{mp}}{N_p} - \dfrac{V_{mp}}{N_s R_p}}{\dfrac{V_{mp}}{N_s} - R_s \dfrac{I_{mp}}{N_p}} \qquad (21)$$

R_D is the dynamic resistance of the p–n junction or differential resistance of the diode when the cell is operating at its maximum power and is determined as follows:

$$R_D = \left.\frac{dV_D}{dI_D}\right|_{P=P_m} = \frac{n V_t}{I_0 \exp\left(\dfrac{1}{n V_t}\left(\dfrac{V_{mp}}{N_s} + R_s \dfrac{I_{mp}}{N_p}\right)\right)} \qquad (22)$$

3.3.2 Cost Function Expression. By rearranging Eq. (17), we obtain the following expression:

$$(R_s + R_p)I_{sc} = N_p R_p (I_{ph} + I_s)\left(1 - \frac{I_s}{(I_{ph} + I_s)}\exp\left(\frac{R_s I_{sc}}{N_p n V_T}\right)\right) \qquad (23)$$

Which can be put in the form

$$I_0 \exp\left(\frac{R_s I_{sc}}{N_p n V_T}\right) = (I_{ph} + I_s) - \frac{(R_s + R_p)}{N_p R_p}I_{sc} \qquad (24)$$

One intrinsic property of most photovoltaic cells is that the value of $\exp\left(\dfrac{R_s I_{sc}}{N_p n V_T}\right) \approx 0$. Thus, Eq. (23) can be reduced to

$$I_{sc} \approx \frac{N_p R_p}{(R_s + R_p)}(I_{ph} + I_s) \qquad (25)$$

By differentiating Eq. (6), we can obtain the following Eq. (26):

$$\frac{dV}{dI} = -\left(\frac{N_s}{N_p}\right)\frac{1 + R_s\left[\dfrac{I_0}{n V_t}\exp\left(\dfrac{1}{n V_t}\left(\dfrac{V}{N_s} + R_s \dfrac{I}{N_p}\right)\right) + \dfrac{1}{R_p}\right]}{\dfrac{I_0}{n V_t}\exp\left(\dfrac{1}{n V_t}\left(\dfrac{V}{N_s} + R_s \dfrac{I}{N_p}\right)\right) + \dfrac{1}{R_p}} \qquad (26)$$

At the short-circuit point, Eq. (25) becomes

$$\left.\frac{dV}{dI}\right|_{\substack{V=0 \\ I=I_{sc}}} = -\left(\frac{N_s}{N_p}\right)\frac{1 + R_s\left[\dfrac{I_0}{n V_t}\exp\left(\dfrac{R_s I_{sc}}{N_p n V_t}\right) + \dfrac{1}{R_p}\right]}{\dfrac{I_0}{n V_t}\exp\left(\dfrac{R_s I_{sc}}{N_p n V_t}\right) + \dfrac{1}{R_p}} \qquad (27)$$

Substituting Eqs. (24) into (27) yields

$$\left.\frac{dV}{dI}\right|_{\substack{V=0 \\ I=I_{sc}}} = \left(\frac{N_s}{N_p}\right)\frac{(R_s+R_p)(R_sI_{sc}-N_pnV_t)-N_pR_sR_p(I_{ph}+I_0)}{N_pR_p(I_{ph}+I_0)-(R_s+R_p)I_{sc}+N_pnV_t} \tag{28}$$

Combining Eqs. (27) and (28), we obtain

$$\left.\frac{dV}{dI}\right|_{\substack{V=0 \\ I=I_{sc}}} \cong \left(\frac{N_s}{N_p}\right)(R_s+R_p) \tag{29}$$

Finally, the cost function ϕ defined as the difference between the expression in Eq. (28) and that in Eq. (29) can be written as follows:

$$\phi = \left(\frac{N_s}{N_p}\right)\left[\frac{(R_sI_{sc}-N_pnV_T)(R_s+R_p)-N_pR_sR_p(I_{ph}+I_s)}{N_pR_p(I_{ph}+I_s)-(R_s+R_p)I_{sc}+N_pnV_T}\right.$$
$$\left.-(R_s+R_p)\right] \approx 0 \tag{30}$$

3.3.3 Parameter Reduction. To solve Eqs. (16)–(18) and the relation in Eq. (6) which contains five parameters, it is possible to manipulate them to get rid of some parameters so that the solution can be found easily. Because n and R_s are on the exponents, which are difficult to eliminate, only I_{ph}, I_0, and R_p will be eliminated. Thus, combining Eqs. (16)–(18) allows us to estimate I_{ph}, I_0, and R_p, which are given by the following expressions, respectively:

$$I_{ph} = \left(1+\frac{R_s}{R_p}\right)\frac{I_{sc}}{N_p}$$
$$+\frac{\left(I_{sc}+\frac{R_sI_{sc}}{R_p}-\frac{N_p}{N_s}\frac{V_{oc}}{R_p}\right)\left[\exp\left(\frac{R_sI_{sc}}{N_pnV_t}\right)-1\right]}{N_p\left[\exp\left(\frac{V_{oc}}{N_snV_t}\right)-\exp\left(\frac{R_sI_{sc}}{N_pnV_t}\right)\right]} \tag{31}$$

$$I_0 = \frac{I_{sc}+\frac{R_sI_{sc}}{R_p}-\frac{N_p}{N_s}\frac{V_{oc}}{R_p}}{N_p\left[\exp\left(\frac{V_{oc}}{N_snV_t}\right)-\exp\left(\frac{R_sI_{sc}}{N_pnV_t}\right)\right]} \tag{32}$$

$$R_p = \frac{N_sXR_sI_{sc}-N_pXV_{oc}-N_sR_sI_{sc}+N_sR_sI_{mp}+N_pV_{mp}}{N_s(I_{sc}-I_{mp}-XI_{sc})} \tag{33}$$

with

$$X = \frac{\exp\left(\frac{1}{nV_t}\left(\frac{V_{mp}}{N_s}+R_s\frac{I_{mp}}{N_p}\right)\right)-\exp\left(\frac{R_sI_{sc}}{N_pnV_t}\right)}{\exp\left(\frac{V_{oc}}{N_snV_t}\right)-\exp\left(\frac{R_sI_{sc}}{N_pnV_t}\right)} \tag{34}$$

Combining Eqs. (21) and (22), we obtain

$$I_o\exp\left(\frac{1}{nV_t}\left(\frac{V_{mp}}{N_s}+R_s\frac{I_{mp}}{N_p}\right)\right) = \frac{nV_t\left(\frac{I_{mp}}{N_p}+\frac{R_s}{R_p}\frac{I_{mp}}{N_p}-\frac{V_{mp}}{N_sR_p}\right)}{\frac{V_{mp}}{N_s}-R_s\frac{I_{mp}}{N_p}} \tag{35}$$

Let

$$I_o\exp\left(\frac{1}{nV_t}\left(\frac{V_{mp}}{N_s}+R_s\frac{I_{mp}}{N_p}\right)\right)$$
$$= \frac{nV_t(N_sR_sI_{mp}+N_sR_pI_{mp}-N_pV_{mp})}{R_p(N_pV_{mp}-N_sR_sI_{mp})} \tag{36}$$

Furthermore, subtracting Eq. (17) from Eq. (18) and neglecting $\exp\left(\frac{R_sI_{sc}}{N_pnV_t}\right)$, we obtain

$$I_o\exp\left(\frac{1}{nV_t}\left(\frac{V_{mp}}{N_s}+R_s\frac{I_{mp}}{N_p}\right)\right) = \left(1+\frac{R_s}{R_p}\right)\left(\frac{I_{sc}}{N_p}-\frac{I_{mp}}{N_p}\right)-\frac{V_{mp}}{N_sR_p} \tag{37}$$

A second explicit form of R_p is obtained from Eqs. (36) and (37) and is given by

$$R_p = \frac{N_p^2V_{mp}^2+N_s^2R_s^2I_{mp}(I_{sc}-I_{mp})+N_sN_pR_s(N_snV_tI_{mp}-I_{sc}V_{mp})-N_sN_p^2nV_tV_{mp}}{N_s^2R_sI_{mp}(I_{sc}-I_{mp})+N_sN_pV_{mp}(I_{sc}-I_{mp})-N_s^2N_pnV_tI_{mp}} \tag{38}$$

With Eqs. (33) and (38), R_p can obviously be eliminated and this allows us to establish an autonomous implicit relation for the series resistance R_s represented by

$$R_s = \frac{N_pV_{oc}V_{mp}(I_{sc}-I_{mp})+N_sN_p^2nV_t(I_{sc}V_{mp}-I_{mp}V_{oc})-N_pI_{sc}V_{mp}^2+\frac{N_sN_p^2nV_tV_{mp}(2I_{mp}-I_{sc})}{X}}{N_sN_p(I_{sc}I_{mp}(V_{oc}-V_{mp})-I_{mp}^2V_{oc})} \tag{39}$$

The expression (39) is an equation with two unknowns n and R_s.

3.3.4 Reduced New Form Procedure. The NRF algorithm is a loop of search processes. Each loop is mainly composed of three steps and a procedure to find n for the next loop, as shown in Fig. 3.

The search starts with $n=+1.0$; it ends when the ten-thousandth digit of n is found. Since some solar cells display a relatively high n, its value is generated in the selected range of 1–7. This choice ensured accurate extraction of n for almost all types of solar cells and modules [58,59]. First, the P–V parameters (V_m, I_m, V_{oc}, and I_{sc}) were calculated from the provided I–V data using polynomial, exponential, and Gaussian curve fits around the points

where P_m, I_{sc}, and V_{oc} are located, respectively. Then, take $n=1.0$ (the smallest plausible value) and step $h=+0.1$; R_s becomes the only variable in (40) that can be written as $\varphi(R_s)=0$. Because of its complex form, solving $\varphi(R_s)=0$ analytically is almost impossible. Therefore, MATLAB's "fzero" solver is used to solve $\varphi(R_s)=0$ and obtain the value of the series resistance R_s. The "fzero" function is based on Brent's algorithm. This algorithm combines the bisection method, the inverse quadratic interpolation method, and the secant method. It is used to determine the zero of a one-dimensional continuous function around a given initial value. The values of R_p, I_0, and I_{ph} are then evaluated using Eqs. (34), (33), and (32), respectively. The cost ϕ is also evaluated using (31) with the obtained
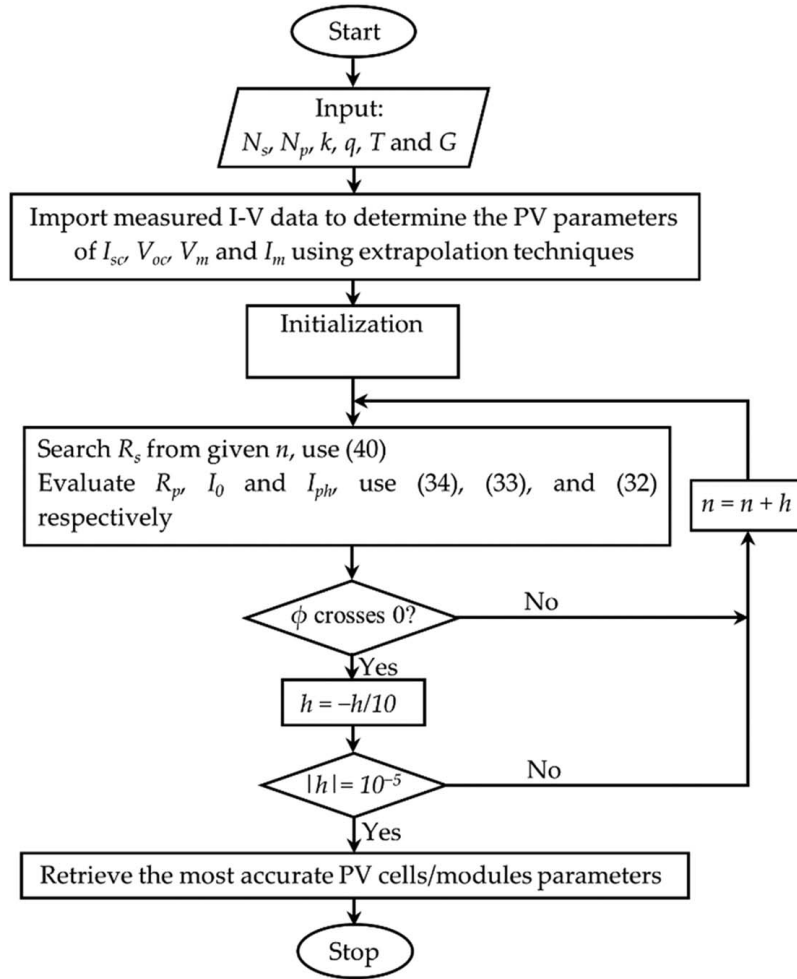
Fig. 3 Searching algorithm of the NRF method

parameters. If ϕ passes through zero (or changes sign), then the actual value of n is between the current and previous values. Then change the direction of the scan and divide h by 10 and then move to the next value of n. Otherwise, change the value of n with the same value of h. Continue scanning until the step h is considerably small (10^{-5}).

3.4 Statistical Errors. In order to evaluate the goodness of fit of the model, the predicted I–V and P–V curves are compared to their experimental counterparts. Based on this comparison, several common performance indicators namely individual absolute errors (IAEC) and (IAEP) on current and power respectively, individual bias errors (IBEC) and (IBEP) on current and power respectively, relative error (RE) and RMSE are calculated

$$\text{IBEC} = I(V_i) - Ith(V_i, p) \tag{40}$$

$$\text{IAEC} = |I(V_i) - Ith(V_i, p)| \tag{41}$$

$$\text{IBEP} = P(V_i) - Pth(V_i, p) \tag{42}$$

$$\text{IAEP} = |P(V_i) - Pth(V_i, p)| \tag{43}$$

$$\text{RE} = \left| \frac{I(V_i) - Ith(V_i, p)}{I(V_i)} \right| \tag{44}$$

$$\text{RMSE} = \sqrt{\frac{1}{N} \sum_{i=1}^{N} [I(V_i) - Ith(V_i, p)]^2} \tag{45}$$

IAEC, IAEP, IBEC, and IBEP are indications of the uncertainty of the estimate. They measure the extent to which the estimated data may differ from their experimental values. The RMSE and RE will provide an appreciation of the overall appearance and point accuracy of the theoretical I–V curves.

3.5 Updating of Electrical Parameters. The parameters of a PV model vary with irradiance and temperature. The expressions (46)–(51) allow us to obtain the new values of the parameters in the real conditions (G, T), from those in the STC conditions (G_{STC}, T_{STC})

$$I_{ph}(G, T) = I_{phSTC}\left[1 + \alpha_{I_{sc}}(T - T_{STC})\right]\left(\frac{G}{G_{STC}}\right) \tag{46}$$

$$I_0(G, T) = I_{0STC}\left(\frac{T}{T_{STC}}\right)^3 \exp\left[\frac{1}{k}\left(\frac{E_{gSTC}}{T_{STC}} - \frac{E_g(T)}{T}\right)\right] \tag{47}$$

$$\frac{E_g(T)}{E_{gSTC}} = 1 - 2,677 \cdot 10^{-4}(T - T_{STC}) \tag{48}$$
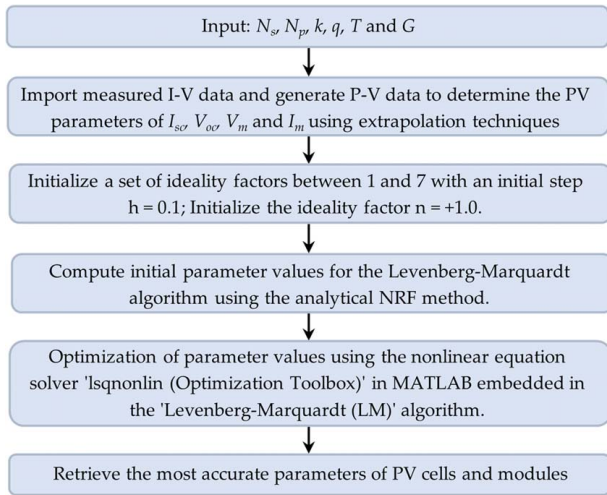
Fig. 4 Methodology adopted for parameters extraction of single-diode model

$$\frac{R_s(G, T)}{R_{sSTC}} = \left(\frac{T}{T_{STC}}\right)\left[1 - 0.217\ln\left(\frac{G}{G_{STC}}\right)\right] \qquad (49)$$

$$\frac{R_{sh}(G, T)}{R_{pSTC}} = \frac{G_{STC}}{G} \qquad (50)$$

$$n = n_{STC}\left(\frac{T}{T_{STC}}\right) \qquad (51)$$

where E_{gSTC} represents the gap of the semiconductor material under STC conditions and α_{Isc} the temperature coefficient for the short-circuit current.

3.6 Procedure for Identifying Photovoltaic Parameters With the ImLM Method. The process of identifying the PV parameters, including initializing the parameters' values through NRF and then optimizing their values through the combined approach of LM and NRF (ImLM), is presented step by step in Fig. 4.

The principle consists in generating the values of V_{mp}, I_{mp}, V_{oc}, and I_{sc} from the measured or digitized I–V data which will be used as starting values for the program. Then, the LM algorithm is used to estimate the model parameters. Note that LM requires initial values of the parameters more or less close to the optimal solution. These are estimated by the NRF method. Indeed, an incorrect initial value or far from the optimal solution can affect the accuracy of the algorithm, its convergence and its convergence speed as reported by Refs. [60,61]. The proposed approach (ImLM) is expected to help improve the accuracy of the LM method and save valuable computation time. The obtained optimal parameter values are used to generate simulated I–V data for each device type. The RMSE is then calculated and compared to those obtained by other recent methods reported in the literature.

4 Results and Discussions

To validate the performance of ImLM in solving the 1DM5P model parameter extraction problem, ImLM is applied on five PV devices with various characteristics. The details of these characteristics are presented in Table 1.

The proposed ImLM method is compared to several well-known methods used for the estimation of the five 1DM model parameters, including parameters identification of PV model using Improved slime mould optimizer and Lambert W-function (ImSMA) [64], classified perturbation mutation-based particle swarm optimization algorithm (CPMPSO) [43], an enhanced adaptive differential evolution algorithm for parameter extraction of photovoltaic models (EJADE) [65], a performance-guided JAYA algorithm for parameters identification of photovoltaic cell and module (PGJAYA) [66],

Table 1 Details of the characteristics of the PV devices used

PV Devices	Type	Technology	References	Data sources	N_s	N_p	G (W/m²)	T (°C)
RTC France	Cell	Monocrystalline	[13,31]	Published in the reference	1	1	1000	33
PVM 752 GaAs	Cell	GaAs thin film	[13,58]	Published in the reference	1	1	1000	25
Photowatt-PWP201	Module	Polycrystalline	[31]	Published in the reference	36	1	1000	45
STM6-40/36	Module	Monocrystalline	[13,59]	Published in the reference	36	1	1000	51
STP6-120/36	Module	Polycrystalline	[13,41,62,63]	Published in the reference	36	1	1000	55

Table 2 Comparison of the parameters extracted from the RTC France solar cell

| Method	I_{ph} (A)	I_o (μA)	R_s (Ω)	R_p (Ω)	n	RMSE
ImLM (proposed)	0.7608	0.3107	0.0366	52.8900	1.5177	**7.7301×10^{-4}**
ImSMA	0.7608	0.3223	0.0364	53.8989	1.5215	7.7518×10^{-4}
FFO	0.7609	0.3166	0.0365	53.2724	1.4791	7.9310×10^{-4}
PGJAYA	0.7608	0.3230	0.0364	53.7185	1.4812	9.8602×10^{-4}
MLBSA	0.7608	0.3230	0.0364	53.7185	1.4812	9.8602×10^{-4}
SATLBO	0.7608	0.3232	0.0364	53.7256	1.4812	9.8602×10^{-4}
TLABC	0.7608	0.0323	0.0364	53.7164	1.4812	9.8602×10^{-4}
ITLBO	0.7608	0.3230	0.0364	53.7185	1.4812	9.8602×10^{-4}
EJADE	0.7608	0.3230	0.0364	53.7185	1.4812	9.8602×10^{-4}
ISCE	0.7608	0.3230	0.0364	53.7185	1.4812	9.8602×10^{-4}
EHA-NMS	0.7608	0.3230	0.0364	53.7185	1.4812	9.8602×10^{-4}
Rcr-IJADE	0.7608	0.3230	0.0364	53.7185	1.4812	9.8602×10^{-4}
ELBA	0.7608	0.3230	0.0364	53.7185	1.4812	9.8602×10^{-4}
CPMPSO	0.7608	0.3230	0.0364	53.7185	1.4812	9.8602×10^{-4}
JADE	0.7608	0.3229	0.0364	53.6477	1.4811	9.8606×10^{-4}
GOTLBO	0.7608	0.3316	0.0363	54.1154	1.4838	9.8744×10^{-4}
IJAYA	0.7608	0.3228	0.0364	53.7595	1.4811	9.8603×10^{-3}
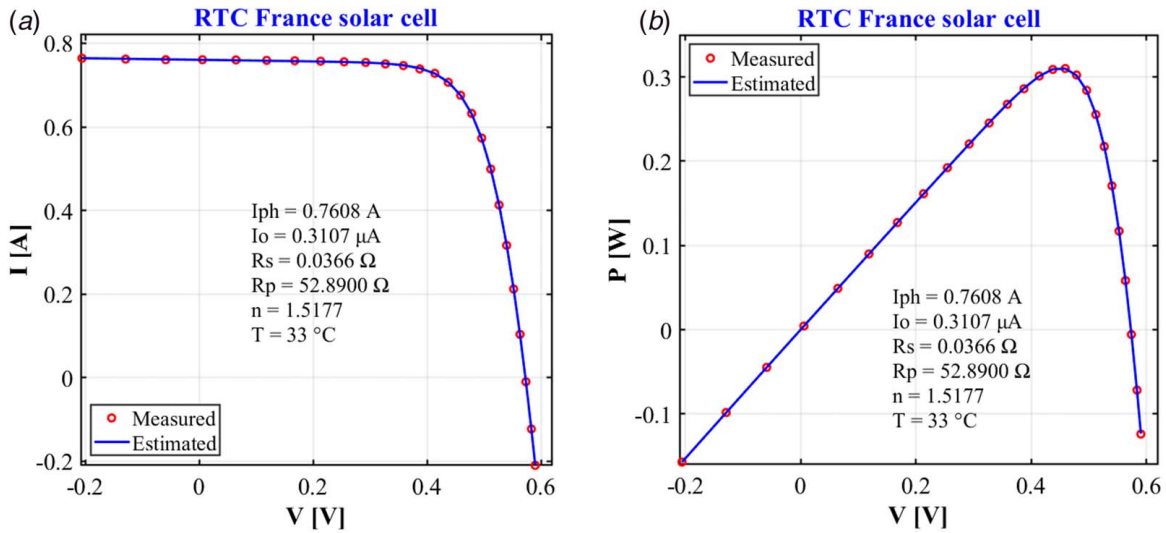
Fig. 5   Comparisons between the measured data and the curves simulated by ImLM for the RTC France silicon cell

improved teaching-learning-based optimization (ITLBO) [62], Multiple learning backtracking search algorithm for estimating parameters of photovoltaic models (MLBSA) [67], parameter extraction of solar cell models using improved shuffled complex evolution algorithm (ISCE) [41], Teaching-learning-based artificial bee colony for solar photovoltaic parameter estimation (TLABC) [68], parameters identification of photovoltaic models using an improved JAYA optimization algorithm (IJAYA) [69], parameters identification of photovoltaic models using self-adaptive teaching-learning-based optimization (SATLBO) [69], parameters identification of solar cell models using generalized oppositional teaching-learning-based optimization (GOTLBO) [70], parameters identification of photovoltaic models using hybrid adaptive Nelder-Mead simplex algorithm based on eagle strategy (EHA-NMS) [71], parameter extraction of solar cell models using repaired adaptive differential evolution (Rcr-IJADE) [72], adaptive differential evolution with optional external archive (JADE) [73], parameter extraction of photovoltaic models using an enhanced Lévy flight bat algorithm (ELBA) [15], Directional Bat Algorithm (DBA) [74], New directional bat algorithm for continuous optimization problems (NBA) [75], Simple and efficient estimation of photovoltaic cells and modules parameters using approximation and correction technique (ACT) [76], Bat algorithm: a novel approach for global engineering optimization (BA) [77], Artificial bee colony (ABC) [55], Backtracking search algorithm (BSA) [78], parameter

extraction of photovoltaic models using an enhanced Lévy flight bat algorithm (ELPSO) [13], electrical characterization of photovoltaic modules using farmland fertility optimizer (FFO) [79], and extracting solar cell model parameters based on chaos particle swarm algorithm (CPSO) [58].

The statistical quantities used for comparison are RMSE and RE. Recall that the smaller the value of RMSE, the more accurate the extracted parameters will be.

4.1   Validation on Photovoltaic Cells. Two photovoltaic cells of different technologies are used in this section to examine the performance and accuracy of the ImLM method. These are the 57 mm diameter commercial silicon solar cell from RTC France and the GaAs thin-film cell, PVM 752. Details of the characteristics of these two PV cells are shown in Table 1.

For the commercial RTC France PV cell, ImLM was compared to several methods with respect to RMSE values. The extracted parameters and corresponding RMSE values for each method are shown in Table 2, where the best RMSE values have been highlighted in bold type.

In Table 2, it can be observed that ImLM recorded the best RMSE value (7.7301×10^{-4}). ImSMA provided the second best result (7.7518×10^{-4}), FFO the third best result (7.9310×10^{-4}) followed by EJADE, PGJAYA, ITLBO, MLBSA, ISCE, TLABC,
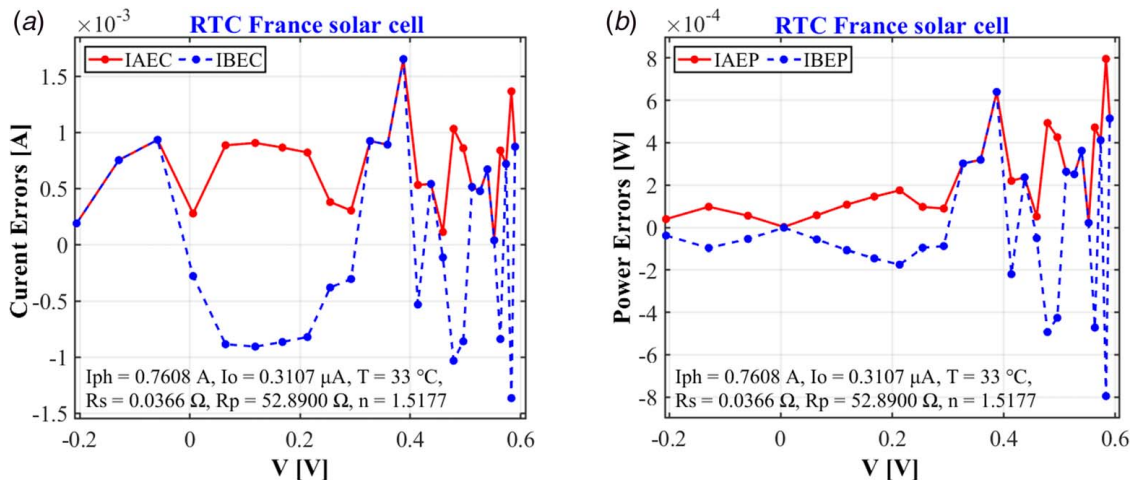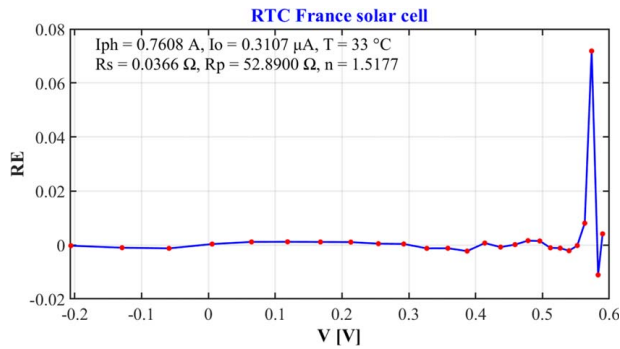

Fig. 6   Individual errors between measured and ImLM estimated data for the RTC France silicon cell

Fig. 7 Relative error between simulated and measured data for the RTC France solar cell

SATLBO, EHA-NMS, Rcr-IJADE, ELBA, and CPMPSO, which show an identical result (9.8602×10^{-4}). The worst result (9.8603×10^{-4}) is obtained by IJAYA. Although the second best RMSE value is close to the best RMSE value, it is significant for any reduction in the objective function. Since the precise parameter values were not available, the smaller the objective function value, the more precise the extracted parameters.

Furthermore, based on the parameters extracted by ImLM, the I–V and P–V curves are shown in Fig. 5. It is clear that the data simulated by ImLM and those measured are highly consistent for the I–V and P–V curves. In addition, IAEC and IAEP as well as IBEC and IBEP, between the simulated and measured data, are presented in Table 9 in the Appendix.

We can infer from Table 9, Figs. 6 and 7 that all the IAEC values do not exceed 1.66×10^{-3} and all the IAEP values are less than 7.97×10^{-3}. Furthermore, all RE values are in the range (-1.11×10^{-2}; 7.19×10^{-2}). Thus, these values are relatively small, which demonstrates the accuracy of the extracted parameters. The actual behavior

of the RTC France P–V cell can therefore be accurately described by the one-diode model.

Following the same procedure as before, the ImLM method was evaluated on the PVM 752 GaAs thin-film cell. After determining the model parameters, the simulated currents were calculated, and the different performance indicators were evaluated. The results obtained by ImLM for this module are compared with those of ten methods as shown in Table 3, in which the best results have been marked in bold.

It is worth mentioning that ImLM outperformed all the stochastic and deterministic optimization methods used for comparison, namely, ELBA, DBA, NBA, BSA, BA, ACT, ELPSO, ABC, and CPSO. Table 4 clearly shows that the best RMSE value is obtained by ImLM (2.0903×10^{-4}), which is slightly better than those obtained by ELBA (2.2780×10^{-4}) and DBA (2.2931×10^{-4}). The poor value of RMSE (2.5400×10^{-2}) is obtained by ELPSO and CPSO. It should be noted that although the differences between the three best RMSE values are very small, they are significant for any reduction in the objective function.

In addition, based on the parameters extracted by ImLM, the I–V, P–V, IAEC, IAEP, IBEC, and IBEP curves are presented in Figs. 8 and 9.

An excellent fit and very good agreement between the simulated and measured data can be observed over the entire voltage range. All IAEC and IAEP values are less than or below 3.2×10^{-3} A and 3.21×10^{-3} W, respectively. In addition, the values of IBEC and IBEP are in the range (-2.47×10^{-3} A, 3.19×10^{-3} A) and (-2.26×10^{-3} W, 3.21×10^{-3} W), respectively.

In addition, Fig. 10 shows all RE values fall in the range (-8.99×10^{-3}, 6.55×10^{-3}) for both current and power. Thus, these values are relatively small, which demonstrates the accuracy of the parameters extracted by the ImLM approach.

4.2 Validation on Photovoltaic Modules. In this section, the proposed ImLM method was tested on three different P–V modules,

**Table 3 Comparison of the parameters extracted from the PVM 752 GaAs thin-film solar cell**

Method	I_{ph} (A)	Io (μA)	R_s (Ω)	R_p (Ω)	n	RMSE
ImLM (proposed)	0.1000	19.4224	0.6165	684	1.7341	**2.0903×10^{-4}**
ELBA	0.1001	0.0000	0.6605	608.01	1.6157	2.2780×10^{-4}
DBA	0.1000	0.0000	0.6582	661.31	1.6241	2.2931×10^{-4}
NBA	0.1000	0.0000	0.5957	1000.00	1.8010	3.9469×10^{-4}
ACT	0.1000	19.4231	0.6166	684.52	1.7341	7.7894×10^{-4}
ABC	0.1033	32.0000	0.5000	100.00	1.7742	2.0412×10^{-3}
BSA	0.1039	84.9000	0.5000	100.00	1.8586	2.1469×10^{-3}
BA	0.0911	38.3591	0.2179	789.91	1.7996	8.6007×10^{-3}
ELPSO	0.1150	0.0000	0.1591	14.43	1.7686	2.5400×10^{-2}
CPSO	0.1165	0.0000	0.3466	14.24	1.6171	2.5400×10^{-2}

Table 4 Comparison of the extracted optimal parameters of the Photowatt-PWP201 module

Method	I_{ph} (A)	I_o (μA)	R_s (Ω)	R_p (Ω)	n	RMSE
ImLM (proposed)	1.0324	2.5027	0.0345	20.8127	1.3169	**2.0400×10^{-3}**
CPMPSO	1.0305	3.4823	1.2013	27.2773	1.3512	2.4251×10^{-3}
ISCE	1.0305	3.4823	0.0334	27.2773	1.3512	2.4251×10^{-3}
EHA-NMS	1.0305	3.4823	0.0334	27.2773	1.3512	2.4251×10^{-3}
Rcr-IJADE	1.0305	3.4823	0.0334	27.2773	1.3512	2.4251×10^{-3}
IJAYA	1.0305	3.4703	0.0334	27.1493	1.3508	2.4251×10^{-3}
PGJAYA	1.0305	3.4818	0.0334	27.2737	1.3512	2.4251×10^{-3}
MLBSA	1.0305	3.4823	0.0334	27.2773	1.3512	2.4251×10^{-3}
SATLBO	1.0305	3.4827	0.0334	27.2890	1.3512	2.4251×10^{-3}
GOTLBO	1.0305	3.4991	0.0334	27.4914	1.3517	2.4251×10^{-3}
TLABC	1.0306	3.4715	0.0334	27.0260	1.3509	2.4251×10^{-3}
ITLBO	1.0305	3.4823	0.0334	27.2773	1.3512	2.4251×10^{-3}
JADE	1.0305	3.4831	0.0334	27.2868	1.3512	2.4251×10^{-3}
EJADE	1.0305	3.4823	0.0334	27.2773	1.3512	2.4251×10^{-3}
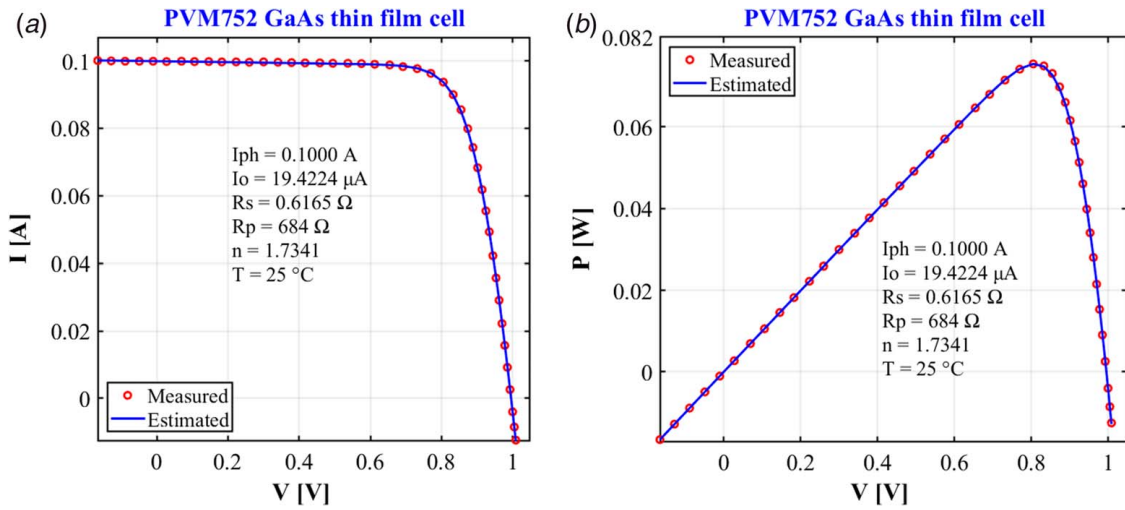
Fig. 8 Comparisons between the measured data and the curves simulated by ImLM for PVM 752 GaAs thin-film cell
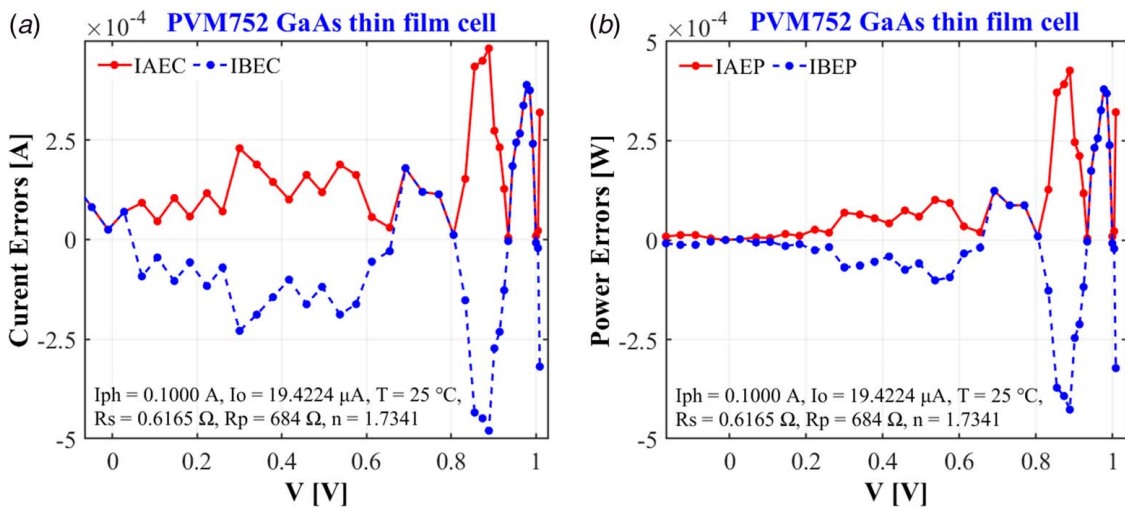
Fig. 9 Individual errors between measured and ImLM estimated data for PVM 752 GaAs thin-film cell

including Photowatt-PWP-201 module, STM6-40/36 module, and STP6-120/36 module. The RMSE value obtained by ImLM on each tested module was compared with those obtained by CPMPSO, EJADE, PGJAYA, ITLBO, ISCE, MLBSA, TLABC, IJAYA, SATLBO, EHA-NMS, GOTLBO, Rcr-IJADE, and JADE methods. The extracted parameters and RMSE obtained by each of the tested methods are presented in Tables 4–6.

For these three P–V modules, the proposed ImLM method obtained the lowest RMSE values. Therefore, ImLM can extract the single-diode model parameters more efficiently and accurately than the methods used in the study.

As for the photovoltaic cells, the optimal parameters obtained by the ImLM method for each of the three modules are used to plot the I–V and P–V curves. The IAEC, IAEP, IBEC, and IBEP errors were also calculated to indicate the deviation between the simulated data and the experimental data. The results of the calculations are presented in Tables 11–13 in the Appendix. In the same context, the results are plotted and presented in Figs. 11–16.

Analysis of these figures indicates excellent agreement and good correlation between the experimental and estimated data for each of the three modules tested. Furthermore, for each of the Photowatt-PWP-201, STM6-40/36, and STP6-120/36 modules, the evolution of RE values as a function of voltage is shown in Figs. 17–19, respectively.

All the RE values, both for current and for power, are in the range $(-1.75 \times 10^{-2}, 1.88 \times 10^{-2})$ for each of the three modules. Thus, these values are relatively small, demonstrating the accuracy of the extracted parameters.

4.3 Simulation of the Electrical Behavior of Modules Under Different Environmental Conditions.. To further investigate its
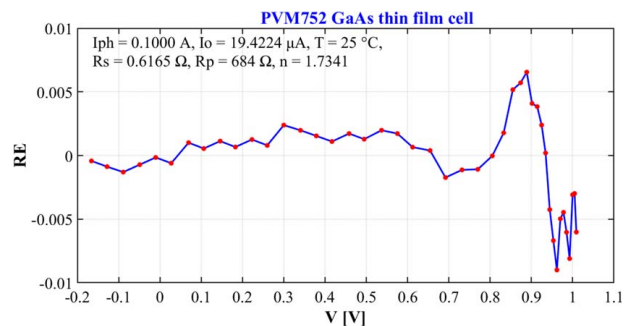
Fig. 10 Relative error between simulated and measured data for the PVM 752 GaAs thin-film solar cell

Table 5   Comparison of the extracted optimal parameters of the STM6-40/36 module

| Method	I_{ph} (A)	I_o (μA)	R_s (Ω)	Rp [Ω]	n	RMSE
ImLM (proposed)	1.6639	1.7412	0.0043	15.9313	1.5205	**1.7219×10^{-3}**
EJADE	1.6639	1.7387	0.0043	15.9283	1.5203	1.7298×10^{-3}
GOTLBO	1.6639	1.7387	0.0043	15.9283	1.5203	1.7298×10^{-3}
ITLBO	1.6639	1.7387	0.0043	15.9283	1.5203	1.7298×10^{-3}
MLBSA	1.6639	1.7387	0.0043	15.9283	1.5203	1.7298×10^{-3}
PGJAYA	1.6639	1.7389	0.0043	15.9290	1.5203	1.7298×10^{-3}
SATLBO	1.6639	1.7387	0.0043	15.9283	1.5203	1.7298×10^{-3}
TLABC	1.6639	1.7387	0.0043	15.9283	1.5203	1.7298×10^{-3}
EHA-NMS	1.6639	1.7387	0.0043	15.9283	1.5203	1.7298×10^{-3}
ISCE	1.6639	1.7387	0.0043	15.9283	1.5203	1.7298×10^{-3}
Rcr-IJADE	1.6639	1.7387	0.0043	15.9283	1.5203	1.7298×10^{-3}
CPMPSO	1.6639	1.7387	0.0043	15.9283	1.5203	1.7298×10^{-3}
JADE	1.6638	1.7946	0.0042	16.0190	1.5238	1.7324×10^{-3}
IJAYA	1.6637	1.8353	0.0040	15.9449	1.5263	1.7548×10^{-3}

Table 6   Comparison of the extracted optimal parameters of the STP6-120/36 module

Method	I_{ph} (A)	Io (μA)	R_s (Ω)	R_p (Ω)	n	RMSE
ImLM(proposed)	7.4752	1.9369	0.0047	15.9361	1.2447	**1.4251×10^{-2}**
CPMPSO	7.4725	2.3350	0.0046	22.2199	1.2601	1.6601×10^{-2}
ISCE	7.4725	2.3350	0.0046	22.2200	1.2601	1.6601×10^{-2}
EHA-NMS	7.4725	2.3350	0.0046	22.2200	1.2601	1.6601×10^{-2}
Rcr-IJADE	7.4725	2.3350	0.0046	22.2200	1.2601	1.6601×10^{-2}
PGJAYA	7.4725	0.0000	0.0046	22.2200	1.2601	1.6601×10^{-2}
MLBSA	7.4725	2.3350	0.0046	22.2200	1.2601	1.6601×10^{-2}
SATLBO	7.4725	2.3350	0.0046	22.2200	1.2601	1.6601×10^{-2}
GOTLBO	7.4725	2.3350	0.0046	22.2200	1.2601	1.6601×10^{-2}
TLABC	7.4725	2.3349	0.0046	22.2100	1.2601	1.6601×10^{-2}
ITLBO	7.4725	2.3350	0.0046	22.2200	1.2601	1.6601×10^{-2}
EJADE	7.4725	2.3350	0.0046	22.2200	1.2601	1.6601×10^{-2}
IJAYA	7.4672	2.2536	0.0046	27.5900	1.2571	1.6731×10^{-2}
JADE	7.4645	3.4139	0.0044	1439.70	1.2926	1.7430×10^{-2}

practicability, the proposed method is used in this section to simulate the behavior of three PV modules of different technologies under all environmental conditions. These are SM55 (monocrystalline), KC200GT (multi-crystalline), and ST40 (thin film). For this purpose, the proposed approach is first used to extract the parameters (Iph_{STC}, I_{0STC}, Rs_{STC}, Rp_{STC}, and n_{STC}) of the single-diode model for each of the three PV modules under the reference conditions (STC) using the I–V characteristics provided by the manufacturers. Then, using Eqs. (46)–(51), the values of the parameters (Iph, I_0, Rs, Rp, n) under operational conditions (G, T) are derived and are used to simulate the I–V and P–V curves of the different modules tested. These I–V and P–V curves are compared to those published by the module manufacturers. The experimental data used for the comparison are obtained by digitizing the I–V curves given in the manufacturers' data sheets.
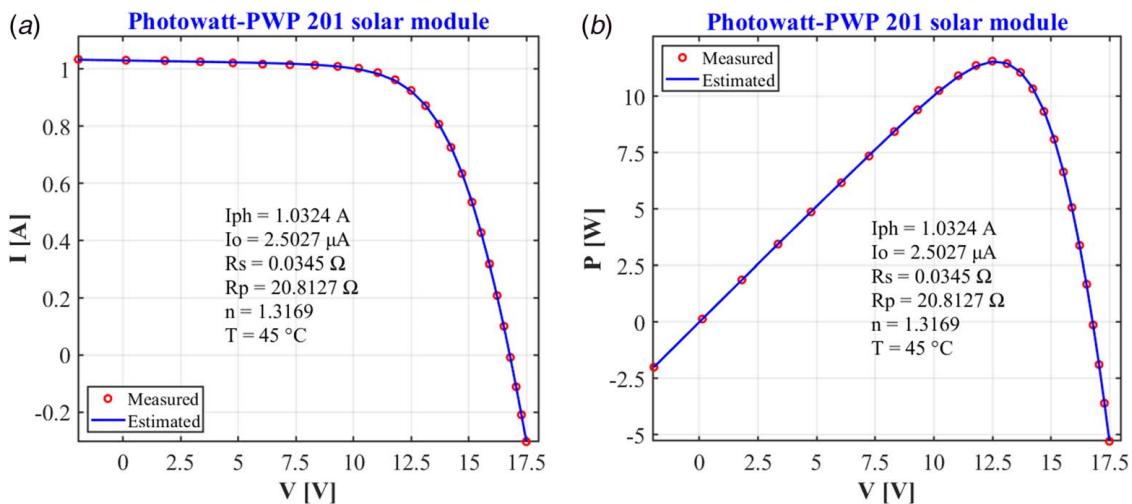
Fig. 11   Comparisons between the measured data and the curves simulated by ImLM for the photowatt-PWP201 polycrystalline silicon module
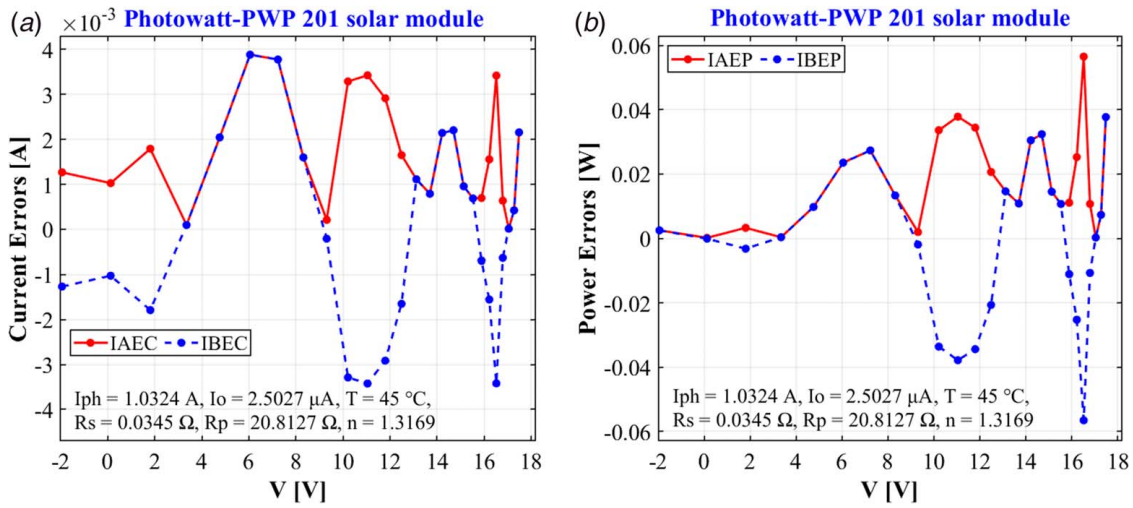
Fig. 12 Individual errors between measured and lmLM estimated data for the photowatt-PWP201 polycrystalline silicon module
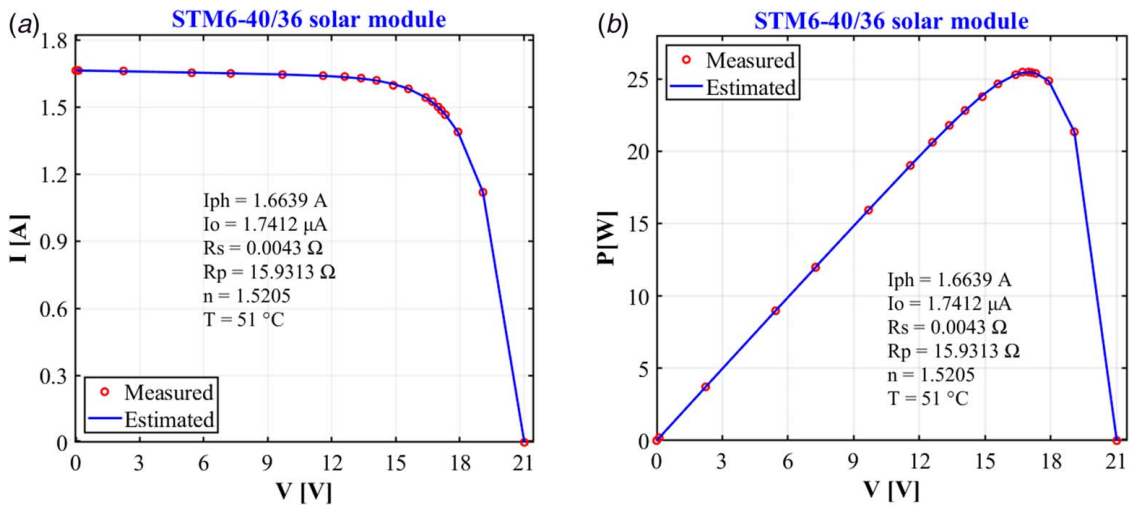

Fig. 13 Comparisons between the measured data and the curves simulated by lmLM for the STM6-40/36 monocrystalline silicon module
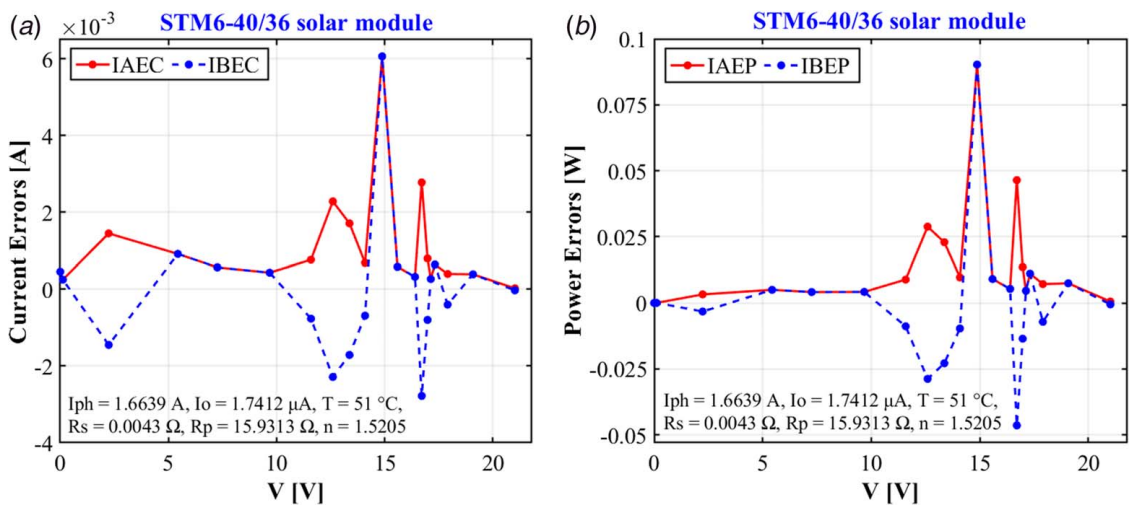
Fig. 14 Individual errors between measured and lmLM estimated data for the STM6-40/36 monocrystalline silicon module
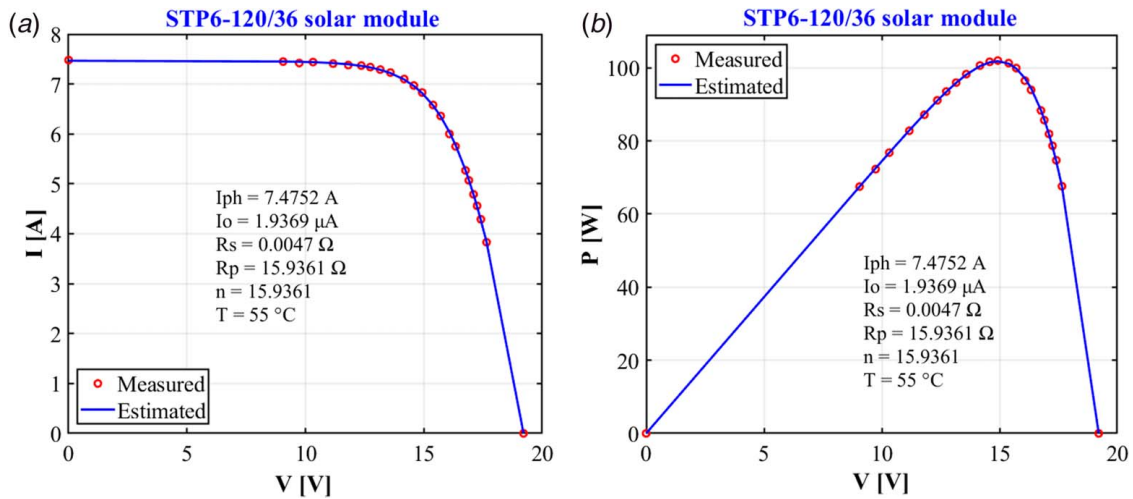
Fig. 15 Comparisons between the measured data and the curves simulated by ImLM for the STP6-120/36 polycrystalline silicon module
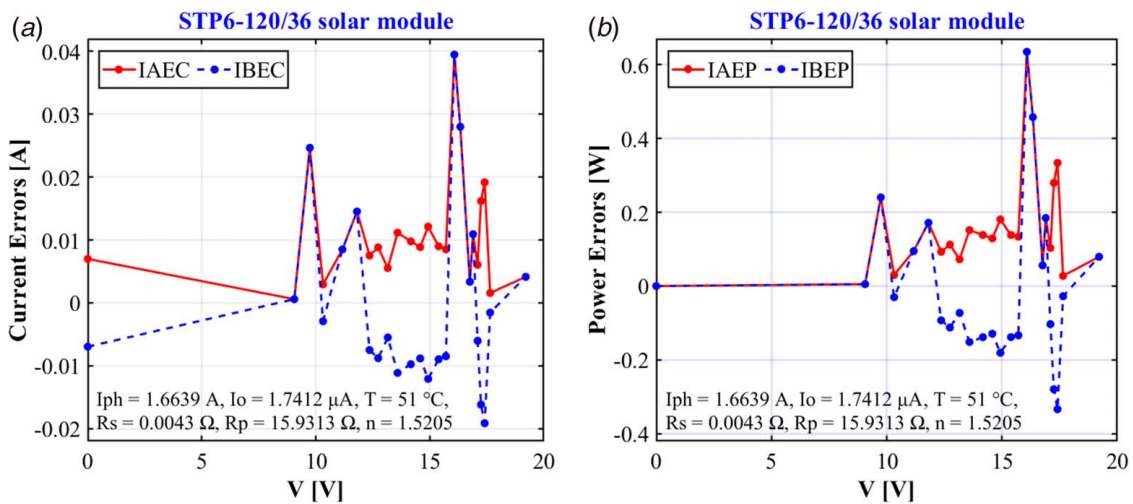
Fig. 16 Individual errors between measured and ImLM estimated data for the STP6-120/36 polycrystalline silicon module

4.3.1 Irradiation Analysis. In this section, the proposed approach is used to simulate the impact of varying solar irradiance at a given temperature on the behavior of a PV module. The estimated parameters, of the three PV modules, at different irradiance levels (1000 W/m^2, 800 W/ m^2, 600 W/m^2, 400 W/m^2 and 200 W/m^2) and at a constant temperature (25 °C) as well as the RMSE values are provided in Table 7.

The electric current is then estimated and shown in Figs. 20–22 for each module. Analysis of these results reveals an excellent fit between the simulated and experimental I–V data. In addition, the ImLM approach could achieve low RMSE values when used to simulate the I–V characteristics at various irradiations. The impact of increasing irradiance on the electrical behavior of PV modules is clearly visible. Indeed, V_{oc}, I_{sc}, and P_{max} simultaneously
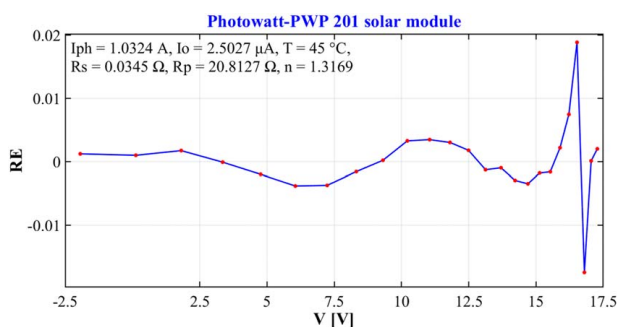
Fig. 17 Relative error between simulated and measured current data for the Photowatt-PWP 201 module

Fig. 18 Relative error between simulated and measured current data for the STM6-40/36 module

Fig. 19 Relative error between simulated and measured current data for the STP6-120/36 module

Fig. 20 Comparison between the estimated model and the experimental data of thin-film ST40 at different irradiance

Fig. 21 Comparison between the estimated model and the experimental data of monocrystalline SM55 at different irradiance

increased with solar irradiance. The performances of the different PV modules have therefore improved following the increase in irradiance; this is reflected in the increase of the photogenerated current I_{ph}.

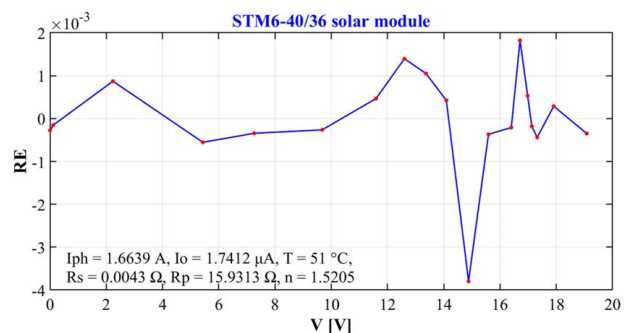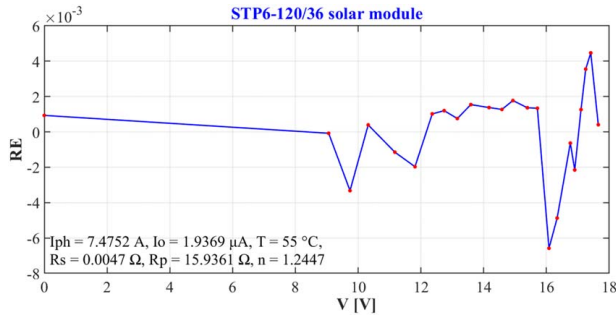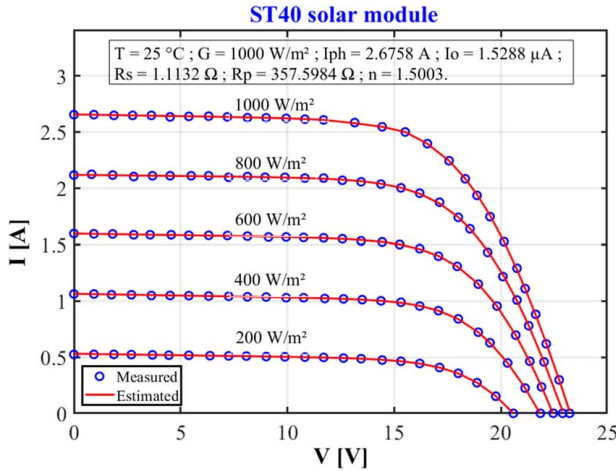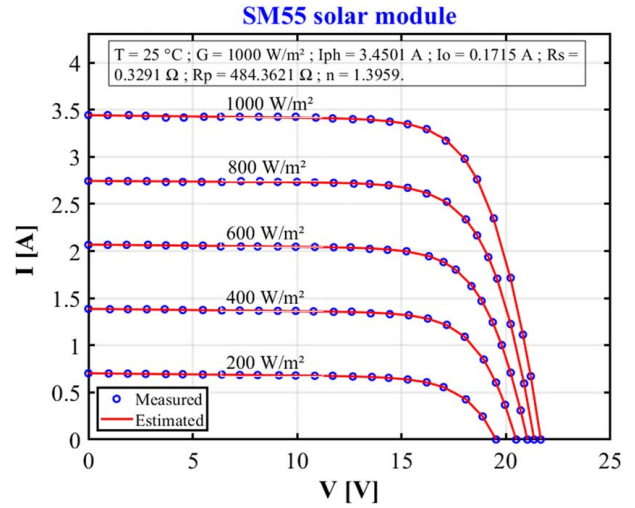*4.3.2 Temperature Analysis.* For this evaluation, the PV modules were considered at different temperatures and at a fixed irradiance of 1000 W/m^2. The parameter values and RMSE values obtained at different temperatures are summarized in Table 8.

Furthermore, the simulated and experimental I–V data at different temperatures are presented in Figs. 23–25. The analysis of these results showed excellent agreement between the simulated and experimental I–V curves over the entire range of voltage records. Therefore, the proposed approach can simulate the electrical behavior of PV modules at different temperatures with competitive accuracy. In addition, an increase in module temperature resulted in a decrease in V_{oc} and a slight increase in the value of I_{sc}. The observed temperature-dependent decrease in V_{oc} can be attributed to the reduced ability of the p–n junction to separate electrons from holes in the photogenerated pairs. Conversely, the increase in I_{sc} can be attributed to the enhanced charge transport and increased generation current I_0. Also, the increase in temperature caused a decrease in the ideality factor, suggesting an improvement in the quality of charge transport in the semiconductor active layer of the modules. These results are considered to be in good agreement with theoretical results and experimental observations [58,80].

Therefore, it can be inferred from these two studies that the simulation results are largely consistent with those obtained by other simulation methods [43,46,66,81]. Therefore, the proposed approach can be used as a competitive model to simulate the electrical behavior of PV cells and modules under different environmental conditions.

Table 7 The extracted parameters for three different types of PV modules by ImLM at different radiation and 25 °C

PV Module	Irradiance (W/m^2)	I_{ph} (A)	I_o (μA)	R_s (Ω)	R_p (Ω)	n	RMSE
Thin film	1000	2.6758	1.5288	1.1132	357.5984	1.5003	7.3434×10^{-4}
ST40	800	2.1380	1.1581	1.1253	332.8889	1.4731	7.7405×10^{-4}
	600	1.6048	1.4419	1.1126	347.6947	1.4958	6.7411×10^{-4}
	400	1.0675	1.8487	1.0806	362.5145	1.5245	6.3077×10^{-4}
	200	0.5331	1.4297	1.1857	344.9832	1.4975	4.7721×10^{-4}
Monocrystalline	1000	3.4501	0.1715	0.3291	484.3621	1.3959	1.1462×10^{-3}
SM55	800	2.7604	0.1439	0.3376	459.8227	1.3811	6.6856×10^{-4}
	600	2.0709	0.1558	0.3304	450.3085	1.3877	8.2394×10^{-4}
	400	1.3828	0.1005	0.3966	427.1129	1.3521	7.0760×10^{-4}
	200	0.6915	0.1465	0.2864	448.2315	1.3807	3.2067×10^{-4}
Multi-crystalline	1000	8.2169	0.0022	0.3438	763.5351	1.0764	1.5391×10^{-3}
KC200GT	800	6.5713	0.0010	0.3573	743.5235	1.0353	1.6313×10^{-3}
	600	4.9343	0.0039	0.3373	743.0016	1.1040	1.2978×10^{-3}
	400	3.2878	0.0015	0.3536	752.0894	1.0550	1.4262×10^{-3}
	200	1.6462	0.0005	0.3811	690.1466	1.0032	1.4186×10^{-3}

Table 8 The extracted parameters of the three photovoltaic modules using ImLM at different temperature and irradiance of 1000 W/m²

PV Module	Temperature	I_{ph} (A)	Io (μA)	R_s (Ω)	R_p (Ω)	n	RMSE
Thin film	25 °C	2.6758	1.5288	1.1132	357.5984	1.5003	7.3434×10^{-4}
ST40	40 °C	2.6809	5.6661	1.1293	364.1098	1.4765	1.3212×10^{-3}
	55 °C	2.6920	18.6807	1.1496	295.0218	1.4498	1.8232×10^{-3}
	70 °C	2.6923	87.5219	1.1259	367.7532	1.4806	7.7771×10^{-4}
Monocrystalline	25 °C	3.4501	0.1715	0.3291	484.3621	1.3959	1.1462×10^{-3}
SM55	40 °C	3.4694	1.0677	0.3175	521.2453	1.4114	3.4653×10^{-3}
	60 °C	3.4946	6.9103	0.3187	484.9674	1.4052	3.7804×10^{-3}
Multi-crystalline	25 °C	3.4501	0.1715	0.3291	484.3621	1.3959	1.1462×10^{-3}
KC200GT	40 °C	3.4694	1.0677	0.3175	521.2453	1.4114	3.4653×10^{-3}
	60 °C	3.4946	6.9103	0.3187	484.9674	1.4052	3.7804×10^{-3}
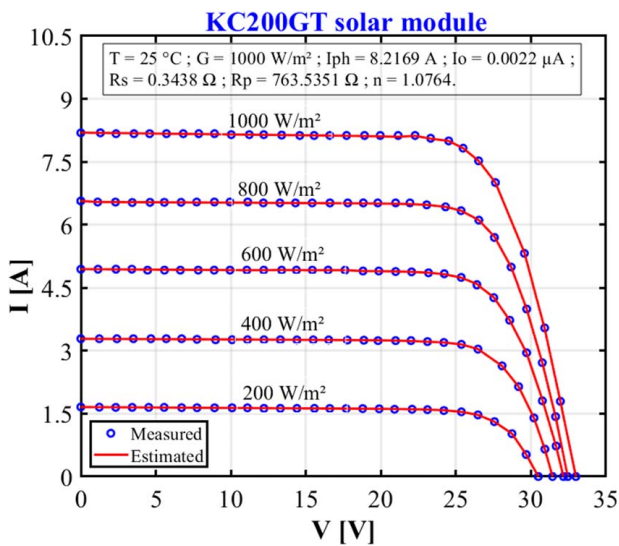
Fig. 22 Comparison between the estimated model and the experimental data of multi-crystalline KC200GT at different irradiance
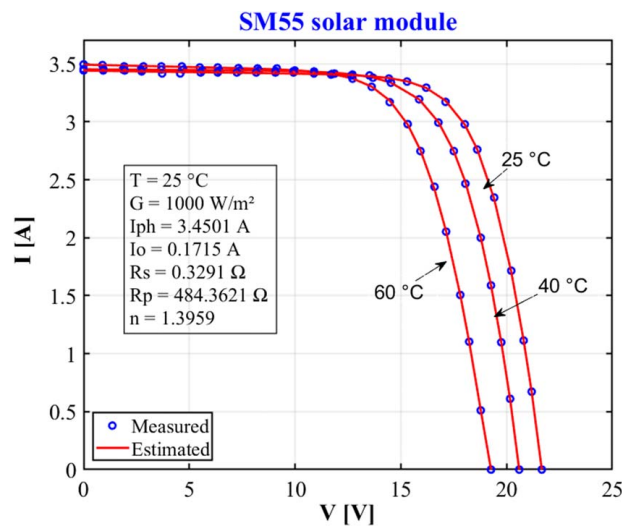
Fig. 24 Comparison between the estimated model and the experimental data of monocrystalline SM55 at different temperature
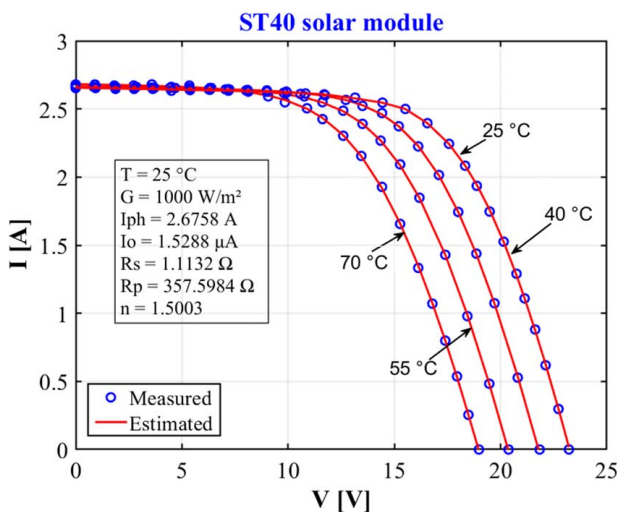
Fig. 23 Comparison between the estimated model and the experimental data of thin-film ST40 at different temperature
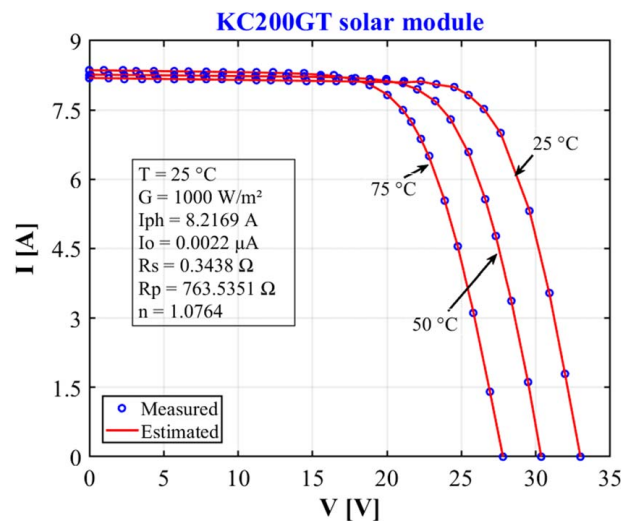
Fig. 25 Comparison between the estimated model and the experimental data of multi-crystalline KC200GT at different temperature

5 Conclusion

In this study, an improved variant of the Levenberg–Marquardt algorithm is proposed to estimate the parameters of solar cell models and PV modules and simulate their electrical behavior under all environmental conditions quickly and accurately. The proposed algorithm combines in a very simple way the Levenberg–Marquardt algorithm and a semi-analytical method called new reduced form. Its performance is examined in detail on single-diode and PV module model parameter estimation problems and compared to various published methods. The experimental and comparative results show that the proposed algorithm can extract the parameters accurately and efficiently and is better than or at least comparable to other published algorithms in the literature. In addition, the tests performed on three PV modules of different types at different irradiation levels and temperature values also suggest that the proposed algorithm is effective and practical. In summary, the proposed approach performs potentially well in solving the single-diode model parameter extraction problem and in simulating I(V) under different conditions. For this reason, the algorithm can serve as a new alternative method for PV cell/module parameter estimation. In the future, it will be discussed to improve the ideality factor evaluation technique and to extend the method to the estimation of the two-diode model parameters.

Conflict of Interest

There are no conflicts of interest.

Data Availability Statement

The data and information that support the findings of this article are freely available.

Appendix

Nomenclature

k = constant of Boltzmann (J/K)
m = number of points of the I–V curve measured
n = ideality factor in real conditions
q = elementary electric charge (C)
G = solar irradiation in real condition (W/m2)
H = Hessian of the function f
T = solar cells temperature in real conditions (K)
n_{STC} = ideality factor in STC conditions
$r(p)$ = residuals vector
E_g = gap of the semiconductor material in the real conditions (eV)
E_{gSTC} = gap of the semiconductor material in STC (eV)
G_{STC} = solar irradiation in STC (W/m^2)
I_0 = saturation current in real conditions (A)
I_{ph} = photocurrent in real conditions (A)
I_{phSTC} = photocurrent in STC conditions (A)
I_{0STC} = saturation current in STC conditions (A)
R_p = shunt resistance in real operating conditions (Ω)
R_{pSTC} = shunt resistance in STC conditions (Ω)
R_s = series resistance in real operating conditions (Ω)
R_{sSTC} = series resistance in STC conditions (Ω)
T_{STC} = solar cells temperature in STC conditions (K)
$f(p)$ = modulus of the vector $r(p)$
Ii = measured current (A)
$Ithi$ = estimated current (A)
$J(p)$ = Jacobian of the vector r(p)

Greek Symbols

α_{Isc} = temperature coefficient of the short-circuit current (A/°C)
λ = damping factor
φ = function of variable n and R_s
ϕ = cost function

Abbreviation

SIAE = Sum of individual absolute error (A)

Table 9   IAE and IBE of ILM for the RTC France monocrystalline silicon solar cell

Item	Measured data			Simulated current data			Simulated power data		
	V (V)	I (A)	P (W)	I_{sim} (A)	IBEC (A)	IAEC (A)	P_{sim} (W)	IBEP (W)	IAEP (W)
1	−0.2057	0.7640	−0.1572	0.7642	1.8924×10^{-4}	1.8924×10^{-4}	−0.1572	-3.8930×10^{-5}	3.8930×10^{-5}
2	−0.1291	0.7620	−0.0984	0.7628	7.5231×10^{-4}	7.5231×10^{-4}	−0.0985	-9.7120×10^{-5}	9.7120×10^{-5}
3	−0.0588	0.7605	−0.0447	0.7614	9.3346×10^{-4}	9.3346×10^{-4}	−0.0448	-5.4890×10^{-5}	5.4890×10^{-5}
4	0.0057	0.7605	0.0043	0.7602	-2.7708×10^{-4}	2.7708×10^{-4}	0.0043	-1.5800×10^{-6}	1.5800×10^{-6}
5	0.0646	0.7600	0.0491	0.7591	-8.8458×10^{-4}	8.8458×10^{-4}	0.0490	-5.7140×10^{-5}	5.7140×10^{-5}
6	0.1185	0.7590	0.0899	0.7581	-9.0569×10^{-4}	9.0569×10^{-4}	0.0898	-1.0732×10^{-4}	1.0732×10^{-4}
7	0.1678	0.7580	0.1272	0.7571	-8.6443×10^{-4}	$8.6443 \cdot 10^{-4}$	0.1270	-1.4505×10^{-4}	1.4505×10^{-4}
8	0.2132	0.7570	0.1614	0.7562	-8.2008×10^{-4}	8.2008×10^{-4}	0.1612	-1.7484×10^{-4}	1.7484×10^{-4}
9	0.2545	0.7555	0.1923	0.7551	-3.7913×10^{-4}	3.7913×10^{-4}	0.1922	-9.6490×10^{-5}	9.6490×10^{-5}
10	0.2924	0.7540	0.2205	0.7537	-3.0353×10^{-4}	3.0353×10^{-4}	0.2204	-8.8750×10^{-5}	8.8750×10^{-5}
11	0.3269	0.7505	0.2453	0.7514	9.2254×10^{-4}	9.2254×10^{-4}	0.2456	3.0158×10^{-4}	3.0158×10^{-4}
12	0.3585	0.7465	0.2676	0.7474	8.9056×10^{-4}	8.9056×10^{-4}	0.2679	3.1927×10^{-4}	3.1927×10^{-4}
13	0.3873	0.7385	0.2860	0.7402	1.6523×10^{-3}	1.6523×10^{-4}	0.2867	6.3993×10^{-4}	6.3993×10^{-4}
14	0.4137	0.7280	0.3012	0.7275	-5.3105×10^{-4}	5.3105×10^{-4}	0.3010	-2.1969×10^{-4}	2.1969×10^{-4}
15	0.4373	0.7065	0.3090	0.7070	5.4038×10^{-4}	5.4038×10^{-4}	0.3092	2.3631×10^{-4}	2.3631×10^{-4}
16	0.4590	0.6755	0.3101	0.6754	-1.1171×10^{-4}	1.1171×10^{-4}	0.3100	-5.1280×10^{-5}	5.1280×10^{-5}
17	0.4784	0.6320	0.3023	0.6310	-1.0311×10^{-3}	$1.0311 \cdot 10^{-3}$	0.3019	-4.9329×10^{-4}	4.9329×10^{-4}
18	0.4960	0.5730	0.2842	0.5721	-8.5873×10^{-4}	8.5873×10^{-4}	0.2838	-4.2593×10^{-4}	4.2593×10^{-4}
19	0.5119	0.4990	0.2554	0.4995	5.1394×10^{-4}	5.1394×10^{-4}	0.2557	2.6308×10^{-4}	2.6308×10^{-4}

Table 9 *Continued*

Item	Measured data			Simulated current data			Simulated power data		
	V (V)	I (A)	P (W)	I_{sim} (A)	IBEC (A)	IAEC (A)	P_{sim} (W)	IBEP (W)	IAEP (W)
20	0.5265	0.4130	0.2174	0.4135	4.7620×10^{-4}	4.7620×10^{-4}	0.2177	2.5072×10^{-4}	2.5072×10^{-4}
21	0.5398	0.3165	0.1708	0.3172	6.7045×10^{-4}	6.7045×10^{-4}	0.1712	3.6191×10^{-4}	3.6191×10^{-4}
22	0.5521	0.2120	0.1170	0.2120	3.8350×10^{-4}	3.8350×10^{-5}	0.1171	2.1170×10^{-5}	2.1170×10^{-5}
23	0.5633	0.1035	0.0583	0.1027	-8.3834×10^{-4}	8.3834×10^{-4}	0.0578	-4.7224×10^{-4}	4.7224×10^{-4}
24	0.5736	−0.0100	−0.0057	−0.0093	7.1851×10^{-4}	7.1851×10^{-4}	−0.0053	4.1214×10^{-4}	4.1214×10^{-4}
25	0.5833	−0.1230	−0.0717	−0.1244	-1.3649×10^{-3}	1.3649×10^{-3}	−0.0725	-7.9614×10^{-4}	7.9614×10^{-4}
26	0.5900	−0.2100	−0.1239	−0.2091	8.7223×10^{-4}	8.7223×10^{-4}	−0.1234	5.1462×10^{-4}	5.1462×10^{-4}
SIAE						$\mathbf{1.8341 \times 10^{-2}}$			$\mathbf{6.6414 \times 10^{-3}}$

Table 10 IAE and IBE of ILM for the PVM 752 GaAs thin-film cell

Item	Measured data			Simulated current data			Simulated power data		
	V (V)	I (A)	P (W)	I_{sim} (A)	IBEC (A)	IAEC (A)	P_{sim} (W)	IBEP (W)	IAEP (W)
1	−0.1659	0.1001	−0.0166	0.1002	5.1770×10^{-5}	5.1770×10^{-5}	−0.0166	-8.5900×10^{-6}	8.5900×10^{-6}
2	−0.1281	0.1000	−0.0128	0.1001	9.6560×10^{-5}	9.6560×10^{-5}	−0.0128	-1.2370×10^{-5}	1.2370×10^{-5}
3	−0.0888	0.0999	−0.0089	0.1000	1.3915×10^{-5}	1.3915×10^{-5}	−0.0089	-1.2360×10^{-5}	1.2360×10^{-5}
4	−0.0490	0.0999	−0.0049	0.1000	8.1020×10^{-5}	8.1020×10^{-5}	−0.0049	-3.9700×10^{-6}	3.9700×10^{-6}
5	−0.0102	0.0999	−0.0010	0.0999	2.4340×10^{-5}	2.4340×10^{-5}	−0.0010	-2.5000×10^{-7}	2.5000×10^{-7}
6	0.0275	0.0998	0.0027	0.0999	6.9280×10^{-5}	6.9280×10^{-5}	0.0027	1.9100×10^{-6}	1.9100×10^{-6}
7	0.0695	0.0999	0.0069	0.0998	-9.2070×10^{-5}	9.2070×10^{-5}	0.0069	-6.4000×10^{-6}	6.4000×10^{-6}
8	0.1061	0.0998	0.0106	0.0998	-4.5530×10^{-5}	4.5530×10^{-5}	0.0106	-4.8300×10^{-6}	4.8300×10^{-6}
9	0.1460	0.0998	0.0146	0.0997	-1.0382×10^{-4}	1.0382×10^{-4}	0.0146	-1.5160×10^{-5}	1.5160×10^{-5}
10	0.1828	0.0997	0.0182	0.0996	-5.7570×10^{-5}	5.7570×10^{-5}	0.0182	-1.0520×10^{-5}	1.0520×10^{-5}
11	0.2230	0.0997	0.0222	0.0996	-1.1630×10^{-4}	1.1630×10^{-4}	0.0222	-2.5930×10^{-5}	2.5930×10^{-5}
12	0.2600	0.0996	0.0259	0.0995	-7.0360×10^{-5}	7.0360×10^{-5}	0.0259	-1.8290×10^{-5}	1.8290×10^{-5}
13	0.3001	0.0997	0.0299	0.0995	-2.2897×10^{-4}	2.2897E-04	0.0299	-6.8710×10^{-5}	6.8710×10^{-5}
14	0.3406	0.0996	0.0339	0.0994	-1.8822×10^{-4}	1.8822×10^{-4}	0.0339	-6.4110×10^{-5}	6.4110×10^{-5}
15	0.3789	0.0995	0.0377	0.0994	-1.4438×10^{-4}	1.4438×10^{-4}	0.0376	-5.4710×10^{-5}	5.4710×10^{-5}
16	0.4168	0.0994	0.0414	0.0993	-1.0025×10^{-4}	1.0025×10^{-4}	0.0414	-4.1780×10^{-5}	4.1780×10^{-5}
17	0.4583	0.0994	0.0456	0.0992	-1.6223×10^{-4}	1.6223×10^{-4}	0.0455	-7.4350×10^{-5}	7.4350×10^{-5}
18	0.4949	0.0993	0.0491	0.0992	-1.1855×10^{-4}	1.1855×10^{-4}	0.0491	-5.8670×10^{-5}	5.8670×10^{-5}
19	0.5370	0.0993	0.0533	0.0991	-1.8806×10^{-4}	$1.880 \times \cdot 10^{-4}$	0.0532	-1.0099×10^{-4}	1.0099×10^{-4}
20	0.5753	0.0992	0.0571	0.0990	-1.6185×10^{-4}	1.6185×10^{-4}	0.0570	-9.3110×10^{-5}	9.3110×10^{-5}
21	0.6123	0.0990	0.0606	0.0989	-5.5890×10^{-5}	5.5890×10^{-5}	0.0606	-3.4220×10^{-5}	3.4220×10^{-5}
22	0.6546	0.0988	0.0647	0.0988	-2.9650×10^{-5}	2.9650×10^{-5}	0.0647	-1.9410×10^{-5}	1.9410×10^{-5}
23	0.6918	0.0983	0.0680	0.0985	1.7903×10^{-4}	1.7903×10^{-4}	0.0681	1.2385×10^{-4}	1.2385E-04
24	0.7318	0.0977	0.0715	0.0978	1.1933×10^{-4}	1.1933×10^{-4}	0.0716	8.7320×10^{-5}	8.7320×10^{-5}
25	0.7702	0.0963	0.0742	0.0964	1.1322×10^{-4}	1.1322×10^{-4}	0.0743	8.7200×10^{-5}	8.7200×10^{-5}
26	0.8053	0.0937	0.0755	0.0937	1.1150×10^{-5}	1.1150×10^{-5}	0.0755	8.9800×10^{-6}	8.9800×10^{-6}
27	0.8329	0.0900	0.0750	0.0898	-1.5215×10^{-4}	1.5215×10^{-4}	0.0748	-1.2673×10^{-4}	1.2673×10^{-4}
28	0.8550	0.0855	0.0731	0.0851	-4.3454×10^{-4}	4.3454×10^{-4}	0.0727	-3.7153×10^{-4}	3.7153×10^{-4}
29	0.8738	0.0799	0.0698	0.0795	-4.4913×10^{-4}	4.4913×10^{-4}	0.0694	-3.9245×10^{-4}	3.9245×10^{-4}
30	0.8887	0.0743	0.0660	0.0738	-4.8008×10^{-4}	4.8008×10^{-4}	0.0656	-4.2665×10^{-4}	4.2665×10^{-4}
31	0.9016	0.0683	0.0616	0.0680	-2.7316×10^{-4}	2.7316×10^{-4}	0.0613	-2.4629×10^{-4}	2.4629×10^{-4}
32	0.9141	0.0618	0.0565	0.0616	-2.3152×10^{-4}	2.3152×10^{-4}	0.0563	-2.1163×10^{-4}	2.1163×10^{-4}
33	0.9248	0.0555	0.0513	0.0554	-1.2697×10^{-4}	1.2697×10^{-4}	0.0512	-1.1743×10^{-4}	1.1743×10^{-4}
34	0.9344	0.0493	0.0461	0.0493	-4.2500×10^{-6}	4.2500×10^{-6}	0.0461	-3.9700×10^{-6}	3.9700×10^{-6}
35	0.9445	0.0422	0.0399	0.0424	1.8437×10^{-4}	1.8437×10^{-4}	0.0400	1.7414×10^{-4}	1.7414×10^{-4}
36	0.9533	0.0357	0.0340	0.0359	2.4362×10^{-4}	2.4362×10^{-4}	0.0343	2.3225×10^{-4}	2.3225×10^{-4}
37	0.9618	0.0291	0.0280	0.0294	2.6624×10^{-4}	2.6624×10^{-4}	0.0282	2.5607×10^{-4}	2.5607×10^{-4}
38	0.9702	0.0222	0.0215	0.0225	3.3683×10^{-4}	3.3683×10^{-4}	0.0219	3.2680×10^{-4}	3.2680×10^{-4}
39	0.9778	0.0157	0.0154	0.0161	3.8830×10^{-4}	3.8830×10^{-4}	0.0157	3.7968×10^{-4}	3.7968×10^{-4}
40	0.9852	0.0092	0.0091	0.0096	3.7476×10^{-4}	3.7476×10^{-4}	0.0094	3.6921×10^{-4}	3.6921×10^{-4}
41	0.9926	0.0026	0.0026	0.0028	2.4049×10^{-4}	2.4049×10^{-4}	0.0028	2.3871×10^{-4}	2.3871×10^{-4}
42	0.9999	−0.0040	−0.0040	−0.0040	-8.6100×10^{-6}	8.6100×10^{-6}	−0.0040	-8.6100×10^{-6}	8.6100×10^{-6}
43	1.0046	−0.0085	−0.0085	−0.0085	-2.1750×10^{-5}	2.1750×10^{-5}	−0.0086	-2.1850×10^{-5}	2.1850×10^{-5}
44	1.0089	−0.0124	−0.0125	−0.0127	-3.1910×10^{-4}	3.1910×10^{-4}	−0.0128	-3.2194×10^{-4}	3.2194×10^{-4}
SIAE						$\mathbf{7.2844 \times 10^{-3}}$			$\mathbf{5.2639 \times 10^{-3}}$

Table 11   IAE and IBE of ILM for the Photowatt-PWP201 polycrystalline silicon module

Item	Measured data			Simulated current data			Simulated power data		
	V (V)	I (A)	P (W)	I_{sim} (A)	IBEC (A)	IAEC (A)	P_{sim} (W)	IBEP (W)	IAEP (W)
1	−1.9426	1.0345	−2.0096	1.0332	$−1.2655 \times 10^{-3}$	1.2655×10^{-3}	−2.0072	2.4583×10^{-3}	2.4583×10^{-3}
2	0.1248	1.0315	0.1287	1.0305	$−1.0260 \times 10^{-3}$	1.0260×10^{-3}	0.1286	$−1.2805 \times 10^{-4}$	1.2805×10^{-4}
3	1.8093	1.0300	1.8636	1.0282	$−1.7900 \times 10^{-3}$	1.7900×10^{-3}	1.8603	$−3.2386 \times 10^{-3}$	3.2386×10^{-3}
4	3.3511	1.0260	3.4382	1.0261	9.4810×10^{-5}	9.4810×10^{-3}	3.4385	3.1773×10^{-4}	3.1773×10^{-4}
5	4.7622	1.0220	4.8670	1.0240	$2.0432 \cdot 10^{-3}$	2.0432×10^{-3}	4.8767	9.7302×10^{-3}	9.7302×10^{-3}
6	6.0538	1.0180	6.1628	1.0219	3.8830×10^{-3}	3.8830×10^{-3}	6.1863	2.3507×10^{-2}	2.3507×10^{-2}
7	7.2364	1.0155	7.3486	1.0193	3.7753×10^{-3}	3.7753×10^{-3}	7.3759	2.7320×10^{-2}	2.7320×10^{-2}
8	8.3189	1.0140	8.4354	1.0156	1.5978×10^{-3}	1.5978×10^{-3}	8.4487	1.3292×10^{-2}	1.3292×10^{-2}
9	9.3097	1.0100	9.4028	1.0098	$−2.0876 \times 10^{-4}$	2.0876×10^{-4}	9.4009	$−1.9435 \times 10^{-3}$	1.9435×10^{-3}
10	10.2163	1.0035	10.2521	1.0002	$−3.2882 \times 10^{-3}$	3.2882×10^{-3}	10.2185	$−3.3594 \times 10^{-2}$	3.3594×10^{-2}
11	11.0449	0.9880	10.9124	0.9846	$−3.4236 \times 10^{-3}$	3.4236×10^{-3}	10.8745	$−3.7813 \times 10^{-2}$	3.7813×10^{-2}
12	11.8018	0.9630	11.3651	0.9601	$−2.9133 \times 10^{-3}$	2.9133×10^{-3}	11.3308	$−3.4382 \times 10^{-2}$	3.4382×10^{-2}
13	12.4929	0.9255	11.5622	0.9239	$−1.6497 \times 10^{-3}$	1.6497×10^{-3}	11.5416	$−2.0610 \times 10^{-2}$	2.0610×10^{-2}
14	13.1231	0.8725	11.4499	0.8736	1.1122×10^{-3}	1.1122×10^{-3}	11.4645	1.4595×10^{-2}	1.4595×10^{-2}
15	13.6983	0.8075	11.0614	0.8083	7.8919×10^{-4}	7.8919×10^{-4}	11.0722	1.0811×10^{-2}	1.0811×10^{-2}
16	14.2221	0.7265	10.3324	0.7286	2.1415×10^{-3}	2.1415×10^{-3}	10.3628	3.0457×10^{-2}	3.0457×10^{-2}
17	14.6995	0.6345	9.3268	0.6367	2.2012×10^{-3}	2.2012×10^{-3}	9.3592	3.2356×10^{-2}	3.2356×10^{-2}
18	15.1346	0.5345	8.0894	0.5355	9.5627×10^{-4}	9.5627×10^{-4}	8.1039	1.4473×10^{-2}	1.4473×10^{-2}
19	15.5311	0.4275	6.6395	0.4282	6.8635×10^{-4}	6.8635×10^{-4}	6.6502	1.0660×10^{-2}	1.0660×10^{-2}
20	15.8929	0.3185	5.0619	0.3178	$−6.9550 \times 10^{-4}$	6.9550×10^{-4}	5.0508	$−1.1054 \times 10^{-2}$	1.1054×10^{-2}
21	16.2229	0.2085	3.3825	0.2069	$−1.5548 \times 10^{-3}$	1.5548×10^{-3}	3.3573	$−2.5223 \times 10^{-2}$	2.5223×10^{-2}
22	16.5241	0.1010	1.6689	0.0976	$−3.4188 \times 10^{-3}$	3.4188×10^{-3}	1.6124	$−5.6492 \times 10^{-2}$	5.6492×10^{-2}
23	16.7987	−0.0080	−0.1344	−0.0086	$−6.3578 \times 10^{-4}$	6.3578×10^{-4}	−0.1451	$−1.0680 \times 10^{-2}$	1.0680×10^{-2}
24	17.0499	−0.1110	−1.8925	−0.1110	1.2650×10^{-5}	1.2650×10^{-5}	−1.8923	2.1569×10^{-4}	2.1569×10^{-4}
25	17.2793	−0.2090	−3.6114	−0.2086	4.2140×10^{-4}	4.2140×10^{-4}	−3.6041	7.2816×10^{-3}	7.2816×10^{-3}
26	17.4885	−0.3030	−5.2990	−0.3008	2.1548×10^{-3}	2.1548×10^{-3}	−5.2613	3.7685×10^{-2}	3.7685×10^{-2}
SIAE						$\mathbf{4.3740 \times 10^{-2}}$			$\mathbf{4.7031 \times 10^{-1}}$

Table 12   IAE and IBE of ILM for the STM6-40/36 monocrystalline silicon module

Item	Measured data			Simulated current data			Simulated power data		
	V (V)	I (A)	P (W)	I_{sim} (A)	IBEC (A)	IAEC (A)	P_{sim} (W)	IBEP (W)	IAEP (W)
1	0	1.6630	0	1.6635	4.5761×10^{-4}	4.5761×10^{-4}	0	0	0
2	0.1180	1.6630	0.1962	1.6633	2.5176×10^{-4}	2.5176×10^{-4}	0.1963	2.9710×10^{-5}	2.9710×10^{-5}
3	2.2370	1.6610	3.7157	1.6596	$−1.4486 \times 10^{-3}$	1.4486×10^{-3}	3.7124	$−3.2405 \times 10^{-3}$	3.2405×10^{-3}
4	5.4340	1.6530	8.9824	1.6539	9.1563×10^{-4}	9.1563×10^{-4}	8.9874	4.9755×10^{-3}	4.9755×10^{-3}
5	7.2600	1.6500	11.9790	1.6506	5.6742×10^{-4}	5.6742×10^{-4}	11.9831	4.1195×10^{-3}	4.1194×10^{-3}
6	9.6800	1.6450	15.9236	1.6454	4.3244×10^{-4}	4.3244×10^{-4}	15.9278	4.1860×10^{-3}	4.1860×10^{-3}
7	11.5900	1.6400	19.0076	1.6392	$−7.6435 \times 10^{-4}$	7.6435×10^{-4}	18.9987	$−8.8588 \times 10^{-3}$	8.8588×10^{-3}
8	12.6000	1.6360	20.6136	1.6337	$−2.2840 \times 10^{-3}$	2.2840×10^{-3}	20.5848	$−2.8778 \times 10^{-2}$	2.8778×10^{-2}
9	13.3700	1.6290	21.7797	1.6273	$−1.7114 \times 10^{-4}$	1.7114×10^{-3}	21.7568	$−2.2882 \times 10^{-2}$	2.2882×10^{-2}
10	14.0900	1.6190	22.8117	1.6183	$−6.8572 \times 10^{-4}$	6.8572×10^{-4}	22.8020	$−9.6618 \times 10^{-3}$	9.6618×10^{-3}
11	14.8800	1.5970	23.7634	1.6031	6.0652×10^{-4}	6.0652×10^{-3}	23.8536	9.0250×10^{-2}	9.0250×10^{-2}
12	15.5900	1.5810	24.6478	1.5816	5.8170×10^{-4}	5.8170×10^{-4}	24.6569	9.0687×10^{-3}	9.0687×10^{-3}
13	16.4000	1.5420	25.2888	1.5423	3.2357×10^{-4}	3.2357×10^{-4}	25.2941	5.3066×10^{-3}	5.3066×10^{-3}
14	16.7100	1.5240	25.4660	1.5212	$−2.7787 \times 10^{-3}$	2.7787×10^{-3}	25.4196	$−4.6432 \times 10^{-2}$	4.6432×10^{-2}
15	16.9800	1.5000	25.4700	1.4992	$−7.9746 \times 10^{-4}$	7.9746×10^{-4}	25.4565	$−1.3541 \times 10^{-2}$	1.3541×10^{-2}
16	17.1300	1.4850	25.4381	1.4853	2.6839×10^{-4}	2.6839×10^{-4}	25.4426	4.5975×10^{-3}	4.5975×10^{-3}
17	17.3200	1.4650	25.3738	1.4656	6.4118×10^{-4}	6.4118×10^{-4}	25.3849	1.1105×10^{-2}	1.1105×10^{-2}
18	17.9100	1.3880	24.8591	1.3876	$−3.9886 \times 10^{-4}$	3.9886×10^{-4}	24.8519	$−7.1435 \times 10^{-3}$	7.1435×10^{-3}
19	19.0800	1.1180	21.3314	1.1184	3.9011×10^{-4}	3.9011×10^{-4}	21.3389	7.4432×10^{-3}	7.4432×10^{-3}
20	21.0200	0	0	0	$−2.5910 \times 10^{-5}$	2.5910×10^{-5}	−0.0005	$−5.4456 \times 10^{-4}$	5.4456×10^{-4}
SIAE						$\mathbf{2.1790 \times 10^{-2}}$			$\mathbf{2.8216 \times 10^{-1}}$

Table 13   IAE and IBE of ILM for the STP6-120/36 polycrystalline silicon module

Item	Measured data			Simulated current data			Simulated power data		
	V (V)	I (A)	P (W)	I_{sim} (A)	IBEC (A)	IAEC (A)	P_{sim} (W)	IBEP (W)	IAEP (W)
1	0	7.4800	0	7.4730	$−6.9871 \times 10^{-3}$	6.9871×10^{-3}	0	0	0
2	9.0600	7.4500	67.5022	7.4506	5.7112×10^{-4}	5.7112×10^{-4}	67.5022	5.1743×10^{-3}	5.1743×10^{-3}
3	9.7400	7.4200	72.5110	7.4447	2.4665×10^{-2}	2.4665×10^{-2}	72.5110	2.4024×10^{-1}	2.4024×10^{-1}

Table 13 *Continued*

Item	Measured data			Simulated current data			Simulated power data		
	V (V)	I (A)	P (W)	I_{sim} (A)	IBEC (A)	IAEC (A)	P_{sim} (W)	IBEP (W)	IAEP (W)
4	10.3200	7.4400	76.7505	7.4371	-2.9339×10^{-3}	2.9339×10^{-3}	76.7505	-3.0278×10^{-2}	3.0278×10^{-2}
5	11.1700	7.4100	82.8646	7.4185	8.4965×10^{-3}	8.4965×10^{-3}	82.8646	9.4906×10^{-2}	9.4906×10^{-2}
6	11.8100	7.3800	87.3294	7.3945	1.4529×10^{-2}	1.4529×10^{-2}	87.3294	1.7159×10^{-1}	1.7159×10^{-1}
7	12.3600	7.3700	91.0002	7.3625	-7.5221×10^{-3}	7.5221×10^{-3}	91.0002	-9.2973×10^{-2}	9.2973×10^{-2}
8	12.7400	7.3400	93.3994	7.3312	-8.8098×10^{-3}	8.8098×10^{-3}	93.3994	-1.1224×10^{-1}	1.1224×10^{-1}
9	13.1600	7.2900	95.8637	7.2845	$-5.5216 \cdot 10^{-3}$	5.5216×10^{-3}	95.8637	-7.2664×10^{-2}	7.2664×10^{-2}
10	13.5900	7.2300	98.1041	7.2188	-1.1158×10^{-3}	1.1158×10^{-2}	98.1041	-1.5164×10^{-1}	1.5164×10^{-1}
11	14.1700	7.1000	100.4685	7.0902	-9.7764×10^{-3}	9.7764×10^{-3}	100.4685	-1.3853×10^{-1}	1.3853×10^{-1}
12	14.5800	6.9700	101.4934	6.9611	-8.8633×10^{-3}	8.8633×10^{-3}	101.4934	-1.2923×10^{-1}	1.2923×10^{-1}
13	14.9300	6.8300	101.7911	6.8179	-1.2112×10^{-2}	1.2112×10^{-2}	101.7911	-1.8084×10^{-1}	1.8084×10^{-1}
14	15.3900	6.5800	101.1279	6.5710	-8.9896×10^{-3}	8.9896×10^{-3}	101.1279	-1.3835×10^{-1}	1.3835×10^{-1}
15	15.7100	6.3600	99.7820	6.3515	-8.5026×10^{-3}	8.5026×10^{-3}	99.7820	-1.3358×10^{-1}	1.3358×10^{-1}
16	16.0800	6.0000	97.1151	6.0395	3.9495×10^{-2}	3.9495×10^{-2}	97.1151	6.3508×10^{-1}	6.3508×10^{-1}
17	16.3400	5.7500	94.4129	5.7780	2.8022×10^{-2}	2.8022×10^{-2}	94.4129	4.5787×10^{-1}	4.5787×10^{-1}
18	16.7600	5.2700	88.3812	5.2733	3.3433×10^{-3}	3.3433×10^{-3}	88.3812	5.6033×10^{-2}	5.6033×10^{-2}
19	16.9000	5.0700	85.8674	5.0809	1.0914×10^{-2}	1.0914×10^{-2}	85.8674	1.8444×10^{-1}	1.8444×10^{-1}
20	17.1000	4.7900	81.8056	4.7840	-6.0449×10^{-3}	6.0449×10^{-3}	81.8056	-1.0337×10^{-1}	1.0337×10^{-1}
21	17.2500	4.5600	78.3804	4.5438	-1.6207×10^{-2}	1.6207×10^{-2}	78.3804	-2.7957×10^{-1}	2.7957×10^{-1}
22	17.4100	4.2900	74.3551	4.2708	-1.9174×10^{-2}	1.9174×10^{-2}	74.3551	-3.3383×10^{-1}	3.3383×10^{-1}
23	17.6500	3.8300	67.5719	3.8284	-1.5636×10^{-3}	1.5636×10^{-2}	67.5719	-2.7597×10^{-2}	2.7597×10^{-2}
24	19.2100	0	0.0793	0.0041	4.1293×10^{-3}	4.1293×10^{-3}	0.0793	7.9323×10^{-2}	7.9323×10^{-2}
SIAE						2.6833×10^{-1}			3.8493

References

[1] Horoufiany, M., and Ghandhari, R., 2019, "A New Photovoltaic Arrays Fixed Reconfiguration Method for Reducing Effects of One- and Two-Sided Mutual Shading," ASME J. Sol. Energy Eng., **141**(3), p. 031013.

[2] Khaki, M., Shahsavar, A., and Khanmohammadi, S., 2018, "Scenario-Based Multi-objective Optimization of an Air-Based Building-Integrated Photovoltaic/Thermal System," ASME J. Sol. Energy Eng., **140**(1), p. 011003.

[3] Sarper, H., Melnykov, I., and Martínez, L. A., 2021, "Prediction of Daily Photovoltaic Energy Production Using Weather Data and Regression," ASME J. Sol. Energy Eng., **143**(6), p. 064502.

[4] Abbassi, R., Abbassi, A., Heidari, A. A., and Mirjalili, S., 2019, "An Efficient Salp Swarm-Inspired Algorithm for Parameters Identification of Photovoltaic Cell Models," Energy Convers. Manage., **179**, pp. 362–372.

[5] Jakhar, S., Soni, M. S., and Boehm, R. F., 2018, "Thermal Modeling of a Rooftop Photovoltaic/Thermal System With Earth Air Heat Exchanger for Combined Power and Space Heating," ASME J. Sol. Energy Eng., **140**(3), p. 031011.

[6] Baharoon, D. A., Rahman, H. A., Omar, W. Z. W., and Fadhl, S. O., 2015, "Historical Development of Concentrating Solar Power Technologies to Generate Clean Electricity Efficiently—A Review," Renewable Sustainable Energy Rev., **41**, pp. 996–1027.

[7] Dougherty, B. P., Fanney, A. H., and Davis, M. W., 2005, "Measured Performance of Building Integrated Photovoltaic Panels—Round 2," ASME J. Sol. Energy Eng., **127**(3), pp. 314–323.

[8] Gwesha, A. O., Li, P., and Alfulayyih, Y. M., 2021, "Optimization of Fixed Photovoltaic Panel 'Tilt' Angles for Maximal Energy Harvest Considering Year-Around Sky Coverage Conditions," ASME J. Sol. Energy Eng., **143**(2), p. 021002.

[9] Fen, L., Quanquan, Y., Shanxu, D., Jinbin, Z., Nianjun, M., and Zhenghong, C., 2015, "A Novel Model for Daily Energy Production Estimation of Grid-Connected Photovoltaic System," ASME J. Sol. Energy Eng., **137**(3), p. 031013.

[10] Cornaro, C., and Musella, D., 2013, "Comparative Analysis of Crystalline and Double-Junction Amorphous Silicon Modules Performance in Outdoor Conditions," ASME J. Sol. Energy Eng., **135**(3), p. 031022.

[11] Averbukh, M., Ben-Galim, Y., and Uhananov, A., 2013, "Development of a Quick Dynamic Response Maximum Power Point Tracking Algorithm for off-Grid System With Adaptive Switching (On-Off) Control of DC/DC Converter," ASME J. Sol. Energy Eng., **135**(2), p. 031022.

[12] Chiteka, K., Arora, R., Sridhara, S. N., and Enweremadu, C. C., 2021, "Influence of Irradiance Incidence Angle and Installation Configuration on the Deposition of Dust and Dust-Shading of a Photovoltaic Array," Energy, **216**, p. 119284.

[13] Rezaee Jordehi, A., 2018, "Enhanced Leader Particle Swarm Optimisation (ELPSO): An Efficient Algorithm for Parameter Estimation of Photovoltaic (PV) Cells and Modules," Sol. Energy, **159**, pp. 78–87.

[14] Nacar, M., Özer, E., and Yılmaz, A. E., 2021, "A six Parameter Single Diode Model for Photovoltaic Modules," ASME J. Sol. Energy Eng., **143**(1), p. 011012.

[15] Deotti, L. M. P., Pereira, J. L. R., and da Silva Júnior, I. C., 2020, "Parameter Extraction of Photovoltaic Models Using an Enhanced Lévy Flight bat Algorithm," Energy Convers. Manage., **221**(2), p. 113114.

[16] Lo Brano, V., and Ciulla, G., 2013, "An Efficient Analytical Approach for Obtaining a Five Parameters Model of Photovoltaic Modules Using Only Reference Data," Appl. Energy, **111**, pp. 894–903.

[17] Cardenas, A. A., Carrasco, M., Mancilla-David, F., Street, A., and Cardenas, R., 2017, "Experimental Parameter Extraction in the Single-Diode Photovoltaic Model via a Reduced-Space Search," IEEE Trans. Ind. Electron., **64**(2), pp. 1468–1476.

[18] Feng, X., Qing, X., Chung, C. Y., Qiao, H., Wang, X., and Zhao, X., 2016, "A Simple Parameter Estimation Approach to Modeling of Photovoltaic Modules Based on Datasheet Values," ASME J. Sol. Energy Eng., **138**(5), p. 051010.

[19] De Soto, W., Klein, S. A., and Beckman, W. A., 2006, "Improvement and Validation of a Model for Photovoltaic Array Performance," Sol. Energy, **80**(1), pp. 78–88.

[20] Laudani, A., Mancilla-David, F., Riganti-Fulginei, F., and Salvini, A., 2013, "Reduced-Form of the Photovoltaic Five-Parameter Model for Efficient Computation of Parameters," Sol. Energy, **97**, pp. 122–127.

[21] Chin, V. J., Salam, Z., and Ishaque, K., 2015, "Cell Modelling and Model Parameters Estimation Techniques for Photovoltaic Simulator Application: A Review," Appl. Energy, **154**, pp. 500–519.

[22] Premalatha, L., Abd Rahim, N., and Fathi, M., 2016, "Performance Evaluation of Two Photovoltaic Cell Technologies in Fluctuating Weather Conditions, Using EN50530 Test Procedure," ASME J. Sol. Energy Eng., **138**(2), p. 021001.

[23] Nashih, S. K., Fernandes, C. A. F., Torres, J. P. N., Gomes, J., and Costa Branco, P. J., 2016, "Validation of a Simulation Model for Analysis of Shading Effects on Photovoltaic Panels," ASME J. Sol. Energy Eng., **138**(4), p. 044503.

[24] Rasool, F., Drieberg, M., Badruddin, N., and Mahinder Singh, B. S., 2017, "PV Panel Modeling With Improved Parameter Extraction Technique," Sol. Energy, **153**, pp. 519–530.

[25] Xiong, G., Zhang, J., Shi, D., and He, Y., 2018, "Parameter Extraction of Solar Photovoltaic Models Using an Improved Whale Optimization Algorithm," Energy Convers. Manage., **174**, pp. 388–405.

[26] Lun, S. X., Du, C. J., Yang, G. H., Wang, S., Guo, T. T., Sang, J. S., and Li, J. P., 2013, "An Explicit Approximate I–V Characteristic Model of a Solar Cell Based on Padé Approximants," Sol. Energy, **92**, pp. 147–159.

[27] Jain, A., 2004, "Exact Analytical Solutions of the Parameters of Real Solar Cells Using Lambert W-Function," Sol. Energy Mater. Sol. Cells, **81**(2), pp. 269–277.

[28] Lun, S. X., Du, C. J., Guo, T. T., Wang, S., Sang, J. S., and Li, J. P., 2013, "A New Explicit i-v Model of a Solar Cell Based on Taylor's Series Expansion," Sol. Energy, **94**, pp. 221–232.

[29] Bencherif, M., and Brahmi, B. N., 2018, "Accurate Method for Loss Parameter Extraction of Solar Panels," ASME J. Sol. Energy Eng., **140**(2), p. 021007.

[30] Petrone, G., and Spagnuolo, G., 2015, "Parameters Identification of the Single-Diode Model for Amorphous Photovoltaic Panels," Proceedings of the 2015 International Conference on Clean Electrical Power (ICCEP), IEEE, pp. 105–109.

[31] Easwarakhanthan, T., Bottin, J., Bouhouch, I., and Boutrit, C., 1986, "Nonlinear Minimization Algorithm for Determining the Solar Cell Parameters With Microcomputers," Int. J. Sol. Energy, **4**(1), pp. 1–12.

[32] Tossa, A. K., Soro, Y. M., Azoumah, Y., and Yamegueu, D., 2014, "A New Approach to Estimate the Performance and Energy Productivity of Photovoltaic Modules in Real Operating Conditions," Sol. Energy, **110**, pp. 543–560.

[33] Jordehi, A. R., 2016, "Time Varying Acceleration Coefficients Particle Swarm Optimisation (TVACPSO): A New Optimisation Algorithm for Estimating Parameters of PV Cells and Modules," Energy Convers. Manage., 129, pp. 262–274.

[34] Karatepe, E., Boztepe, M., and Colak, M., 2006, "Neural Network Based Solar Cell Model," Energy Convers. Manage., 47(9–10), pp. 1159–1178.

[35] Jamadi, M., Merrikh-Bayat, F., and Bigdeli, M., 2016, "Very Accurate Parameter Estimation of Single- and Double-Diode Solar Cell Models Using a Modified Artificial Bee Colony Algorithm," Int. J. Energy Environ. Eng., 7(1), pp. 13–25.

[36] Louzazni, M., Khouya, A., Amechnoue, K., Gandelli, A., Mussetta, M., and Crăciunescu, A., 2018, "Metaheuristic Algorithm for Photovoltaic Parameters: Comparative Study and Prediction With a Firefly Algorithm," Appl. Sci., 8(3), p. 339.

[37] Askarzadeh, A., and Rezazadeh, A., 2013, "Extraction of Maximum Power Point in Solar Cells Using Bird Mating Optimizer-Based Parameters Identification Approach," Sol. Energy, 90, pp. 123–133.

[38] Abdul Kadir, A. F., Khatib, T., Lii, L. S., and Hassan, E. E., 2019, "Optimal Placement and Sizing of Photovoltaic Based Distributed Generation Considering Costs of Operation Planning of Monocrystalline and Thin-Film Technologies," ASME J. Sol. Energy Eng., 141(1), p. 011017.

[39] Sirjani, R., and Shareef, H., 2016, "Parameter Extraction of Solar Cell Models Using the Lightning Search Algorithm in Different Weather Conditions," ASME J. Sol. Energy Eng., 138(4), p. 041007.

[40] Ridha, H. M., 2020, "Parameters Extraction of Single and Double Diodes Photovoltaic Models Using Marine Predators Algorithm and Lambert W Function," Sol. Energy, 209, pp. 674–693.

[41] Gao, X., Cui, Y., Hu, J., Xu, G., Wang, Z., Qu, J., and Wang, H., 2018, "Parameter Extraction of Solar Cell Models Using Improved Shuffled Complex Evolution Algorithm," Energy Convers. Manage., 157, pp. 460–479.

[42] Chen, X., and Yu, K., 2019, "Hybridizing Cuckoo Search Algorithm With Biogeography-Based Optimization for Estimating Photovoltaic Model Parameters," Sol. Energy, 180, pp. 192–206.

[43] Liang, J., Ge, S., Qu, B., Yu, K., Liu, F., Yang, H., Wei, P., and Li, Z., 2020, "Classified Perturbation Mutation Based Particle Swarm Optimization Algorithm for Parameters Extraction of Photovoltaic Models," Energy Convers. Manage., 203, p. 112138.

[44] Mughal, M. A., Ma, Q., and Xiao, C., 2017, "Photovoltaic Cell Parameter Estimation Using Hybrid Particle Swarm Optimization and Simulated Annealing," Energies, 10(8), p. 1213.

[45] Nunes, H. G. G., Pombo, J. A. N., Mariano, S. J. P. S., Calado, M. R. A., and Felippe de Souza, J. A. M., 2018, "A new High Performance Method for Determining the Parameters of PV Cells and Modules Based on Guaranteed Convergence Particle Swarm Optimization," Appl. Energy, 211, pp. 774–791.

[46] Xu, S., and Wang, Y., 2017, "Parameter Estimation of Photovoltaic Modules Using a Hybrid Flower Pollination Algorithm," Energy Convers. Manage., 144, pp. 53–68.

[47] Nunes, H. G. G., Pombo, J. A. N., Bento, P. M. R., Mariano, S. J. P. S., and Calado, M. R. A., 2019, "Collaborative Swarm Intelligence to Estimate PV Parameters," Energy Convers. Manage., 185, pp. 866–890.

[48] Nunes, H. G. G., Silva, P. N. C., Pombo, J. A. N., Mariano, S. J. P. S., and Calado, M. R. A., 2020, "Multiswarm Spiral Leader Particle Swarm Optimisation Algorithm for PV Parameter Identification," Energy Convers. Manage., 225, p. 113388.

[49] Muhammad, F. F., Yahya, M. Y., Hameed, S. S., Aziz, F., Sulaiman, K., Rasheed, M. A., Ahmad, Z., and Hu, X., 2017, "Employment of Single-Diode Model to Elucidate the Variations in Photovoltaic Parameters Under Different Electrical and Thermal Conditions," PLoS One, 12(8), p. e0182925.

[50] Marco Tina, G., 2017, "Simulation Model of Photovoltaic and Photovoltaic/Thermal Module/String Under Nonuniform Distribution of Irradiance and Temperature," ASME J. Sol. Energy Eng., 139(2), p. 021013.

[51] Bany Mousa, O. M., and Taylor, R. A., 2019, "A Broad Comparison of Solar Photovoltaic and Thermal Technologies for Industrial Heating Applications," ASME J. Sol. Energy Eng., 141(1), p. 011002.

[52] Humada, A. M., Hojabri, M., Mekhilef, S., and Hamada, H. M., 2016, "Solar Cell Parameters Extraction Based on Single and Double-Diode Models: A Review," Renewable Sustainable Energy Rev., 56, pp. 494–509.

[53] Ma, T., Gu, W., Shen, L., and Li, M., 2019, "An Improved and Comprehensive Mathematical Model for Solar Photovoltaic Modules Under Real Operating Conditions," Sol. Energy, 184, pp. 292–304.

[54] Ridha, H. M., Heidari, A. A., Wang, M., and Chen, H., 2020, "Boosted Mutation-Based Harris Hawks Optimizer for Parameters Identification of Single-Diode Solar Cell Models," Energy Convers. Manage., 209, p. 112660.

[55] Oliva, D., Abd El Aziz, M., and Ella Hassanien, A., 2017, "Parameter Estimation of Photovoltaic Cells Using an Improved Chaotic Whale Optimization Algorithm," Appl. Energy, 200, pp. 141–154.

[56] Dkhichi, F., Oukarfi, B., Fakkar, A., and Belbounaguia, N., 2014, "Parameter Identification of Solar Cell Model Using Levenberg–Marquardt Algorithm Combined With Simulated Annealing," Sol. Energy, 110, pp. 781–788.

[57] Chouder, A., and Silvestre, S., 2009, "Analysis Model of Mismatch Power Losses in PV Systems," ASME J. Sol. Energy Eng., 131(2), p. 024504.

[58] Muhammadsharif, F. F., Hashim, S., Hameed, S. S., Ghoshal, S. K., Abdullah, I. K., Macdonald, J. E., and Yahya, M. Y., 2019, "Brent's Algorithm Based New Computational Approach for Accurate Determination of Single-Diode Model Parameters to Simulate Solar Cells and Modules," Sol. Energy, 193, pp. 782–798.

[59] Tong, N. T., and Pora, W., 2016, "A Parameter Extraction Technique Exploiting Intrinsic Properties of Solar Cells," Appl. Energy, 176, pp. 104–115.

[60] Kichou, S., Silvestre, S., Guglielminotti, L., Mora-López, L., and Muñoz-Cerón, E., 2016, "Comparison of Two PV Array Models for the Simulation of PV Systems Using Five Different Algorithms for the Parameters Identification," Renewable Energy, 99, pp. 270–279.

[61] Kata, N., Diouf, D., Soro, Y. M., Darga, A., and Maiga, A. S., 2018, "Module Parameter Extraction and Simulation With LTSpice Software Model in Sub-Saharan Outdoor Conditions," Afr. J. Environ. Sci. Technol., 12(12), pp. 523–531.

[62] Li, S., Gong, W., Yan, X., Hu, C., Bai, D., and Wang, L., 2019, "Parameter Estimation of Photovoltaic Models With Memetic Adaptive Differential Evolution," Sol. Energy, 190, pp. 465–474.

[63] Li, J., Gao, X., Cui, Y., Hu, J., Xu, G., and Zhang, Z., 2020, "Accurate, Efficient and Reliable Parameter Extraction of PEM Fuel Cells Using Shuffled Multi-Simplexes Search Algorithm," Energy Convers. Manage., 206, p. 112501.

[64] El-Fergany, A. A., 2021, "Parameters Identification of PV Model Using Improved Slime Mould Optimizer and Lambert W-Function," Energy Rep., 7, pp. 875–887.

[65] Li, S., Gu, Q., Gong, W., and Ning, B., 2020, "An Enhanced Adaptive Differential Evolution Algorithm for Parameter Extraction of Photovoltaic Models," Energy Convers. Manage., 205, p. 112443.

[66] Yu, K., Qu, B., Yue, C., Ge, S., Chen, X., and Liang, J., 2019, "A Performance-Guided JAYA Algorithm for Parameters Identification of Photovoltaic Cell and Module," Appl. Energy, 237, pp. 241–257.

[67] Yu, K., Liang, J. J., Qu, B. Y., Cheng, Z., and Wang, H., 2018, "Multiple Learning Backtracking Search Algorithm for Estimating Parameters of Photovoltaic Models," Appl. Energy, 226, pp. 408–422.

[68] Chen, X., Xu, B., Mei, C., Ding, Y., and Li, K., 2018, "Teaching–Learning–Based Artificial Bee Colony for Solar Photovoltaic Parameter Estimation," Appl. Energy, 212, pp. 1578–1588.

[69] Yu, K., Liang, J. J., Qu, B. Y., Chen, X., and Wang, H., 2017, "Parameters Identification of Photovoltaic Models Using an Improved JAYA Optimization Algorithm," Energy Convers. Manage., 150, pp. 742–753.

[70] Chen, X., Yu, K., Du, W., Zhao, W., and Liu, G., 2016, "Parameters Identification of Solar Cell Models Using Generalized Oppositional Teaching Learning Based Optimization," Energy, 99, pp. 170–180.

[71] Chen, Z., Wu, L., Lin, P., Wu, Y., and Cheng, S., 2016, "Parameters Identification of Photovoltaic Models Using Hybrid Adaptive Nelder-Mead Simplex Algorithm Based on Eagle Strategy," Appl. Energy, 182, pp. 47–57.

[72] Gong, W., and Cai, Z., 2013, "Parameter Extraction of Solar Cell Models Using Repaired Adaptive Differential Evolution," Sol. Energy, 94, pp. 209–220.

[73] Zhang, J., and Sanderson, A. C., 2009, "JADE: Adaptive Differential Evolution With Optional External Archive," IEEE Trans. Evol. Comput., 13(5), pp. 945–958.

[74] Chakri, A., Khelif, R., Benouaret, M., and Yang, X. S., 2017, "New Directional Bat Algorithm for Continuous Optimization Problems," Expert Syst. Appl., 69, pp. 159–175.

[75] Meng, X. B., Gao, X. Z., Liu, Y., and Zhang, H., 2015, "A Novel bat Algorithm With Habitat Selection and Doppler Effect in Echoes for Optimization," Expert Syst. Appl., 42(17–18), pp. 6350–6364.

[76] Muhammad, F. F., Karim Sangawi, A. W., Hashim, S., Ghoshal, S. K., Abdullah, I. K., Hameed, S. S., and Pandolfi, A., 2019, "Simple and Efficient Estimation of Photovoltaic Cells and Modules Parameters Using Approximation and Correction Technique," PLoS One, 14(5), p. e0216201.

[77] Yang, X., and Hossein Gandomi, A., 2012, "Bat Algorithm: A Novel Approach for Global Engineering Optimization," Eng. Comput., 29(5), pp. 464–483.

[78] Zhang, Y., Ma, M., and Jin, Z., 2020, "Backtracking Search Algorithm With Competitive Learning for Identification of Unknown Parameters of Photovoltaic Systems," Expert Syst. Appl., 160, p. 113750.

[79] Agwa, A. M., El-Fergany, A. A., and Maksoud, H. A., 2020, "Electrical Characterization of Photovoltaic Modules Using Farmland Fertility Optimizer," Energy Convers. Manage., 217, p. 112990.

[80] Chander, S., Purohit, A., Sharma, A., Arvind, Nehra, S. P., and Dhaka, M. S., 2015, "A Study on Photovoltaic Parameters of Mono-Crystalline Silicon Solar Cell With Cell Temperature," Energy Rep., 1, pp. 104–109.

[81] Merchaoui, M., Sakly, A., and Mimouni, M. F., 2018, "Particle Swarm Optimisation With Adaptive Mutation Strategy for Photovoltaic Solar Cell/Module Parameter Extraction," Energy Convers. Manage., 175, pp. 151–163.